Reduced chemical kinetic mechanisms for methane combustion in O_2/N_2 and O_2/CO_2 atmosphere

J. Bibrzycki[1] and T. Poinsot[2]
[1] **Corresponding author: jakub.bibrzycki@polsl.pl, Silesian University of Technology, Institute of Thermal Technology, 22 Konarskiego St., 44-100 Gliwice, Poland**
[2] **Université de Toulouse, IMFT (Institut de Mécanique des Fluides de Toulouse) Allée C. Soula, F-31400 Toulouse, France**

Abstract

Two reduced mechanisms (2S-CM2 and J-L) have been tested for a conventional air-methane combustion. Whereas, existing (2S-CM2 and J-L) schemes and refined ones (2S-CM2-JB2 and J-L-JB) were verified using detailed chemistry computations, for specified oxy-fuel conditions. Results for the air-methane case, obtained for the J-L scheme and for the GRI Mech, are in general in better agreement than those evaluated for the 2S-CM2. Large disagreement between detailed chemistry calculations and results obtained for J-L and 2S-CM2 global schemes, for the oxy-fuel combustion, was found for freely propagating 1D laminar premixed flames. Therefore, two new major schemes were evaluated (2S-CM2-JB2 and J-L-JB). Modified schemes improved the agreement with the detailed mechanism considerably, for both considering compositions of the oxidizer ($X_{O_2}^{oxid} = 0,385/X_{CO_2}^{oxid} = 0,615$ and $X_{O_2}^{oxid} = 0,28/X_{CO_2}^{oxid} = 0,72$).

INTRODUCTION

Carbon dioxide emission reduction has become one of the main concern last years, due to the standpoint of most of scientists, who work on climate change that a direct connection between global temperature increase and anthropogenic greenhouse gases emission exists. Carbon dioxide is a specie, which emission cannot be avoided during combustion of the fuel containing carbon. Therefore, emission reduction can be only done through sequestration. In order to underground storage of CO_2, this specie has to be separated from flue gases, which contain mainly nitrogen, what is a very expensive process. One of the best ways to sequestrate CO_2, is to perform a combustion without nitrogen presence in the oxidizer (oxy-fuel combustion). Nevertheless, the combustion in pure oxygen leads to dangerous temperature and flame speed escalation. In order to keep those two quantities at levels similar to air, a mixing of oxygen with part of flue gases is performed, thus, a mixture containing O_2/CO_2 is used as an oxidizer.

Carbon dioxide has different heat capacity, thermal diffusivity and emissivity in comparison to molecular nitrogen. Therefore, the combustion of the fuel in the oxidizer, containing the same mole fraction of CO_2 as it is found for nitrogen in air, leads to significant parameters changes in comparison with conventional fuel-air combustion [14, 4, 7, 2, 3]. The emissivity of this flame changes due to the fact, that carbon dioxide is a three-atomic gas, which was the main topic of Anderson and Johnsson [4]. Benedetto et al. [2] indicated the decrease of laminar flame speed, while nitrogen was displaced by carbon dioxide. The explanation for this behavior was the higher heat capacity of the CO_2, which decreasing the flame temperature and at the same time the combustion rate. The reaction kinetics undergo alterations when N_2 is displaced by CO_2 in the oxidizer. Favor of CO in CO-CO_2 equilibrium and H_2 in H_2O-H_2 equilibrium was found in higher temperatures ($> 2500K$) during oxy-fuel combustion [3].

A computational fluid dynamics is an important toll for a design and a process optimization. Simulation of full-scale geometry, with millions of cells, requires a large memory and long computational

time. In order to safe time required for simulations significantly, simplified combustion mechanisms are used. Schemes containing two (WD, 2S-CM2) [30, 6], four (J-L) [16] or more [31, 8] reactions can be used to describe the combustion phenomena, however, their accuracy is limited. The mechanisms which are created for a conventional combustion of fuel in air were found not to be satisfying for a oxy-fuel combustion [3, 14], because every detailed mechanism has restricted area of usage.

The aim of the present work was simulations in Cosilab of 0D and 1D methane combustion in the oxidizer containing N_2/O_2 as well as CO_2/O_2. Firstly, the detailed mechanism results comparison for two different compositions of the oxidizer and finding the mole fraction of the carbon dioxide in the oxidizer, which results similar combustion conditions to the conventional combustion, were executed. Next step was testing existing and new (created for oxy-fuel combustion) reduced schemes, where the reference results were obtained for detailed mechanism simulation. The 0D simulations were done using equilibrium calculations and auto-ignition delay times, while 1D computations were performed using freely propagating laminar flames, stretched laminar premixed and diffusion flames.

GENERAL QUANTITIES

Molar and mass species fraction

Mole species fractions can be expressed according to Eq. (1), while mass fractions are given by Eq. (2).

$$X_i = n_i / \sum_i^N n_i \tag{1}$$

$$Y_i = m_i / \sum_i^N m_i \tag{2}$$

Between those two quantities following relationship exists Eq. (3) [23].

$$X_i = Y_i (W / W_i) \tag{3}$$

In Eq. (1) and in Eq. (2) letters n and m denote respectively mole and mass quantities in $kmol$ and kg, whereas W is the molar weight of gas mixture Eq. (4). Index i represents each specie, N determines the total number of species in the gas mixture.

$$W = \sum_i^N W_i \cdot X_i \tag{4}$$

Molar concentrations can be calculated according to Eq. (5) [1]. ρ is a density of the gas mixture.

$$C_i = \rho Y_i / W_i \tag{5}$$

$$\rho = \frac{p}{R_z T} \tag{6}$$

where p and T is respectively the mixture pressure in Pa and the temperature in K, R_z can be evaluated as follow:

$$R_z = \frac{R}{W} \tag{7}$$

where R is universal gas constant in $J/(kmolK)$

Calculations of reactants mole fraction

Composition of the fuel and oxidizer are following:
Fuel: $X_{CH_4} = 1$
Oxidizer: $X_{O_2}^{oxid}$; $X_{inert}^{oxid} = 1 - X_{O_2}^{oxid}$

Species mole numbers in the fuel can be written as [26]:

$$n'_C = 1 \cdot X_{CH_4} = 1 \frac{kmolC}{kmolCH_4}$$

$$n'_{H_2} = 2 \cdot X_{CH_4} = 2 \frac{kmolH_2}{kmolCH_4}$$

A stoichiometric amount of oxygen and oxidizer, which are required for complete combustion of fuel, are evaluated as [26]:

$$n'_{O_2 min} = n'_C + 0,5 \cdot n'_{H_2} = 2 \frac{kmolO_2}{kmolCH_4}$$

$$n'_{oxidmin} = \frac{n'_{O_2min}}{X^{oxid}_{inert}}, \frac{kmoloxid}{kmolCH_4}$$

A real quantity of oxidizer used for combustion can be described as follow [26]:

$$n'_{oxid} = n'_{O_2min} \cdot \lambda, \frac{kmoloxid}{kmolCH_4}$$

where λ is oxidizer excess ratio and is a reciprocal of equivalence ratio ($\lambda = \frac{1}{\phi}$).

Mole amount of oxygen and of inert gas, which participate in combustion, can be calculated as:

$$n'_{O_2} = X^{oxid}_{O_2} \cdot n'_{oxid}, \frac{kmolO_2}{kmolCH_4}$$

$$n'_{inert} = X^{oxid}_{inert} \cdot n'_{oxid}, \frac{kmolinert}{kmolCH_4}$$

Homogenous premixed mixture molar fractions of species, which are required as a boundary conditions in Cosilab, can be derived finally from equation (1).

Quantities related to diffusion flames

Identification of the combustion regime can be done using mixture fraction (z), which calculates the local fuel/oxidizer ratio [23]:

$$z = \frac{1}{\phi_b + 1} \cdot (\phi_b \frac{Y_F}{Y^0_F} - \frac{Y_O}{Y^0_O} + 1) \tag{8}$$

where Y^0_F and Y^0_O are mass fractions of the fuel and oxygen at the boundaries on the fuel and oxidizer side respectively; Y_F and Y_O are local mass fractions of the fuel and oxygen respectively.

The equivalence ratio ϕ_b (Eq. (8)) does not correspond to the global equivalence ratio, but characterizes the local structure of the diffusion flames [23]:

$$\phi_b = s \frac{Y^0_F}{Y^0_O} \tag{9}$$

where s is the mass stoichiometric ratio: [23]:

$$s = \frac{\nu'_O W_O}{\nu'_F W_F} \tag{10}$$

where ν'_O and ν'_F are stoichiometric coefficients of the overall (one-step) reaction corresponding to fuel and oxidizer respectively.

Equation (8) is theoretical and does not account radicals, because is created for one-step mechanism, thus the real flame mixture fraction, for methane combustion, should be calculated from following dependence [23]:

$$z_c = \frac{Z_c - 0}{Y^0_F \cdot W_c / W_{CH_4}} \tag{11}$$

where Z_c is passive scalar defined for the C element and is calculated according to equation below [23]:

$$Z_c = W_c \sum_{k=1}^{N} a_k \frac{Y_k}{W_k} \tag{12}$$

where a_k is the number of C elements in k specie.

CHEMICAL KINETICS

Introduction of methane oxidation mechanisms

In this section particular methane oxidation mechanisms are presented, which were employed in calculations. Three different mechanisms were taken as a basis for further development of mechanisms for CH_4 oxy-fuel combustion: GRI Mech 3.0 [10], Jones-Linstedt (J-L) [16] and 2S-CM2 [6] (Table 1). New developed schemes are presented in Table 2. For existing as well as for new schemes the number of species involved in the flame computation was depended on the composition of the oxidizer. Simulation of methane combustion in the oxidizer composed of N_2/O_2 or of CO_2/O_2 contains no argon, what limits the original GRI Mech number of reactions (325) and species (53). In the case of oxy-fuel combustion simulation apart from argon also nitrogen is not present, thus the reduction of species and reactions (Table 1). Table 3 presents reactions of 2-step and 4-step mechanisms while full specification of Arrhenius parameters (Eq. (13)) for those reactions are presented in Table 5 and Table 6. The full specification of reactions for GRI Mech 3.0 is available online [10].

The reaction rate constant can be expressed according to the Arrhenius equation (Eq. (13)), where A_j is a pre-exponential constant, β_j is a temperature exponent, $-E_j$ is the activation energy of the reaction [23].

$$k_j = A_j T^{\beta_j} exp(\frac{-E_j}{RT}) \tag{13}$$

The reaction rate progress is described as a difference between forward and backward reaction rates [1].

$$r_j = k_f \prod_i^N C_i^{\nu'_i} - k_b \prod_i^N C_i^{\nu''_i} \tag{14}$$

Table 1: The existing chemical schemes used in this study.

Fuel/ oxidizer	Scheme name	Number of species	Number of reactions	Usage reason
CH_4/air	GRI Mech 3.0	52	323	Reference scheme
CH_4/air	2S-CM2	5	2	2-step scheme used in AVBP
CH_4/air	J-L (Jones-Linstedt)	6	4	4-step scheme
$CH_4/O_2/CO_2$	GRI Mech 3.0	34	215	Reference scheme
$CH_4/O_2/CO_2$	2S-CM2	5	2	2-step scheme used in AVBP
$CH_4/O_2/CO_2$	J-L (Jones-Linstedt)	6	4	4-step scheme

Table 2: The new chemical schemes developed in this study.

Fuel/ oxidizer	Scheme name	Number of species	Number of reactions	Usage reason
CH_4/air	2S-CM2-JB1	5	2	Modified with PEA on the rich side
$CH_4/O_2/CO_2$	2S-CM2-JB2	5	2	Modified by JB for oxy-fuel combustion
$CH_4/O_2/CO_2$	2S-CM2-JB3	5	2	Modified with PEA on the rich side
$CH_4/O_2/CO_2$	J-L-JB	6	4	Modified by JB 4-step scheme

Table 3: Number of reactions for 2-step and 4-step reduced mechanisms

Reaction number	2-step mechanisms (2S-CM2, 2S-CM2-JB1, 2S-CM2-JB2, 2S-CM2-JB3)	4-step mechanisms (J-L, J-L-JB)
1	$CH_4 + 1,5O_2 => CO + 2H_2O$	$CH_4 + 0,5O_2 => CO + 2H_2$
2	$CO + 0,5O_2 <=> CO_2$	$CH_4 + H_2O => CO + 3H_2$
3		$H_2 + 0,5O_2 <=> H_2O$
4		$CO + H_2O <=> CO_2 + H_2$

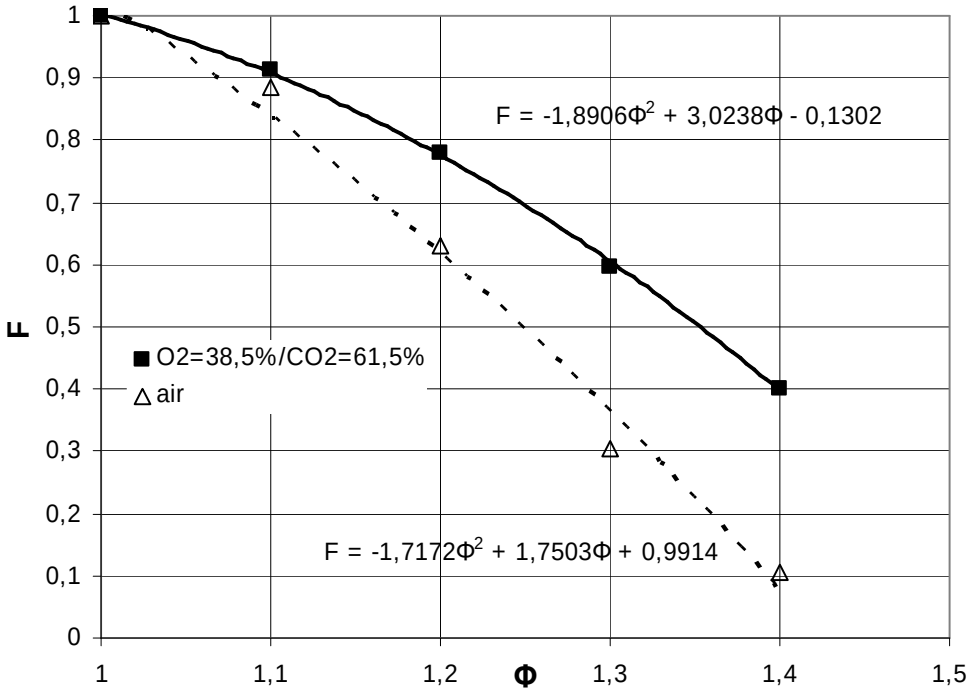

Figure 1: Function F plotted against equivalence ratio for air and $38,5\%O_2/61,5\%CO_2$ cases.

Because the 2-step scheme is not able to predict the laminar flame speed for fuel-rich mixtures, two additional schemes were created (2S-CM2-JB1 and 2S-CM2-JB3) using pre-exponential factor adjustment. Pre-exponential factor adjustment (PEA) is a method of redefining the reaction rate through defining the pre-exponential factor (A) as a function of the local equivalence ratio [11]. In this study it was done through creation of correction functions for both air and $38,5\%O_2/61,5\%CO_2$ cases (Fig. 1). The quantity F presented in Fig. 1 was calculated according to Eq. (15).

$$A = A_0(\frac{{S_L}^2}{{S_{L0}}^2}) = A_0 F \tag{15}$$

where S_L defines the required value of the laminar flame speed, index 0 represents the quantities before readjustment.

For the case with O_2 mole fraction in the oxidizer equal to $0,385$, the function F was evaluated as follow: $F = -1,8906\phi^2 + 3,0238\phi - 0,1302$ and for air case: $F = -1,7172\phi^2 + 1,7503\phi + 0,9914$. Table 4 presents results of calculation of new pre-exponential factors for both reactions (1 and 2) for the 2S-CM2-JB1 and the 2S-CM2-JB3 mechanisms, while full specification of Arrhenius parameters are available in Table 5 and Table 6.

Table 4: Pre-exponential factor values for exemplary fuel-rich mixtures for the 2S-CM2-JB1 2S-CM2-JB3 mechanism; A in cgs

Case	$\phi = 1,1$	$\phi = 1,2$	$\phi = 1,3$	$\phi = 1,4$
A for $O_2 = 0,21; N_2 = 0,79$	$1,68E+15$	$1,24E+15$	$7,29E+14$	$1,52E+14$
A for $O_2 = 0,385; CO_2 = 0,615$	$4,63E+14$	$3,96E+14$	$3,09E+14$	$2,03E+14$

Table 5: Rate constants for the 2S-CM2 scheme and for the modified versions introduced during this work: the activation energies are in cal/mole and the pre-exponential constants in cgs units. Abbreviations $ford$ and *rord* mean forward and reversed order respectively.

Name	2S-CM2	2S-CM2-JB1	2S-CM2-JB2	2S-CM2-JB3
A_1	$2E15$	$(-1,7172\phi^2 + 1,7503\phi + 0,9914)$ $\cdot 2E15$ for $\phi > 1$; $2E15$ for $\phi \in (0;1)$	$5,1E14$	$(-1,8906\phi^2 + 3,0238\phi - 0,1302)$ $\cdot 5,1E14$ for $\phi > 1$; $5,1E14$ for $\phi \in (0;1)$
$n_{1ford}^{CH_4}$	$0,9$	$0,9$	$0,7$	$0,7$
$n_{1ford}^{O_2}$	$1,1$	$1,1$	$1,3$	$1,3$
E_{a1}	35000	35000	35000	35000
A_2	$2E9$	$(-1,7172\phi^2 + 1,7503\phi + 0,9914)$ $\cdot 2E9$ for $\phi > 1$; $2E9$ for $\phi \in (0;1)$	$5,1E8$	$(-1,8906\phi^2 + 3,0238\phi - 0,1302)$ $\cdot 5,1E8$ for $\phi > 1$; $5,1E8$ for $\phi \in (0;1)$
n_{2ford}^{CO}	1	1	1	1
$n_{2ford}^{O_2}$	$0,5$	$0,5$	$0,5$	$0,5$
$n_{2rord}^{CO_2}$	1	1	1	1
E_{a2}	12000	12000	12000	12000

Table 6: Rate constants for the Jones Linstedt scheme and for the modified versions introduced during this work: the activation energies are in $cal/mole$ and the pre-exponential constants in cgs units. Abbreviations $ford$ and *rord* mean forward and reversed order respectively.

J-L	A_1	$n_{1ford}^{CH_4}$	$n_{1ford}^{O_2}$	E_{a1}	A_3	$n_{3ford}^{H_2}$	$n_{3rord}^{H_2}$	$n_{3ford}^{O_2}$	$n_{3rord}^{O_2}$	$n_{3rord}^{H_2O}$	E_{a3}
	$7,824E13$	$0,5$	$1,25$	30000	$1,209E18$	$0,25$	$-0,75$	$1,5$	$1,0$	$1,0$	40000
	A_2	$n_{2ford}^{CH_4}$	$n_{2ford}^{H_2O}$	E_{a2}	A_4	n_{4ford}^{CO}	$n_{4ford}^{H_2O}$	$n_{4rord}^{CO_2}$	$n_{3rord}^{H_2}$	E_{a4}	
	$3,0E11$	$1,0$	$1,0$	30000	$2,75E12$	$1,0$	$1,0$	$1,0$	$1,0$	20000	
J-L-JB	A_1	$n_{1ford}^{CH_4}$	$n_{1ford}^{O_2}$	E_{a1}	A_3	$n_{3ford}^{H_2}$	$n_{3rord}^{H_2}$	$n_{3ford}^{O_2}$	$n_{3rord}^{O_2}$	$n_{3rord}^{H_2O}$	E_{a3}
	$3,5E12$	$0,5$	$1,25$	30000	$3,5E17$	$0,25$	$-0,75$	$1,5$	$1,0$	$1,0$	40000
	A_2	$n_{2ford}^{CH_4}$	$n_{2ford}^{H_2O}$	E_{a2}	A_4	n_{4ford}^{CO}	$n_{4ford}^{H_2O}$	$n_{4rord}^{CO_2}$	$n_{3rord}^{H_2}$	E_{a4}	
	$3,0E11$	$1,0$	$1,0$	30000	$2,75E12$	$1,0$	$1,0$	$1,0$	$1,0$	20000	

Equilibrium reaction modification to irreversible ones in Cosilab

In order to illustrate equilibrium reaction as two irreversible reactions (Table 7), Arrhenius parameters of the reverse reaction have to be known. The derivation of the reverse reaction rate is done by forward reaction rate division by the equilibrium constant at series of temperature from $1000K$ to $3000K$ [1]:

$$k_b = \frac{k_f}{K_c(T)} \tag{16}$$

where K_c can be evaluated from the equilibrium constant related to partial pressures according to equation [1]:

$$K_c = K_p(\frac{p_{atm}}{R \cdot T})^{\Sigma_{i=1}^{N} \nu_i} \tag{17}$$

where ν_i are evaluated as a result of products $\nu_i^{'}$ and reactants $\nu_i^{''}$ stoichiometric coefficient of i specie substraction; equilibrium constant K_p is defined as [1]:

$$K_p = \prod_i^N (\frac{p_i}{p_{atm}})^{\nu_i}$$

where p^0 denotes atmospheric pressure ($1atm$).

Table 7: Reactions of the irreversible 2S-CM2 scheme

Reaction number	Irreversible 2S-CM2
1	$CH_4 + 0,5O_2 => CO + 2H_2$
2	$CO_2 => CO + 0,5O_2$
3	$CO + 0,5O_2 => CO_2$

The two-step (2S-CM2) scheme was investigated in this section. Values of the equilibrium constant related to partial pressures of species was taken from table found in Holman's book [13]. Calculations of the forward reaction rate of the reaction $CO + 0,5O_2 = CO_2$ was done according to equation (13). In order to calculate the backward reaction rate the forward reaction rate has to be described in SI units, therefore, the following equation is used [19]:

$$k_{fSI} = k_{fcgs} \cdot 10^{6 \cdot (1 - \Sigma_{i=1}^{N} \nu_i)} \tag{18}$$

Backward Arrhenius parameters were calculated graphically taking coefficients of linear tendency between $ln(kf/Kc)$ and $1/T$ as it shown in Figure 3. The coefficient next to the inverse of the temperature is equal to $-E_a/R$, while the second one is a natural logarithm of the backward reaction pre-exponential factor (lnA_3) in SI units. To convert SI units of pre-exponential factor (A_3) into cgs a reversed action as described in equation (18) has to be performed. After mathematical transformation of the linear function coefficients and conversion of the Arrhenius parameters into cgs units, the irreversible 2S-CM2 scheme can be introduced into Cosilab. The full specification of the irreversible 2S-CM2 scheme is presented in Table 8.

Computations of the irreversible 2S-CM2 scheme were performed in Cosilab in order to confirm the correctness of backward Arrhenius parameters evaluation. Figure 3 presents temperature, velocity, heat release, reaction rates progress and species profiles for original 2S-CM2 and irreversible schemes. Very good agreement, between those two mechanisms, for presented various quantities, was found. The profile for reaction rate progress ($r3 - r2$) for irreversible 2S-CM2 was calculated through substraction of the reaction rate progress of the reaction 3 and 2.

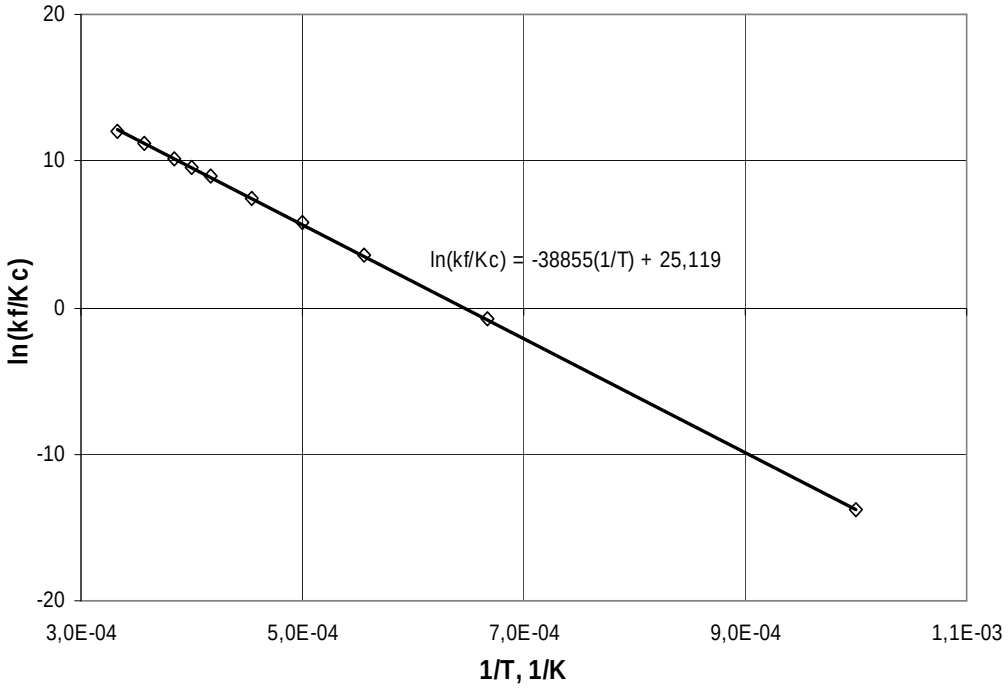

Figure 2: Derivation of the linear function used to calculate backward Arrhenius parameters of $CO + 0,5O_2 <=> CO_2$ reaction from 2S-CM2 scheme.

Table 8: Rate constants for the irreversible 2S-CM2 scheme. Activation energies are in cal/mol and the pre-exponential constants in *cgs* units. Abbreviations $ford$ and *rord* mean forward and reversed order respectively.

A_1	$n_{1ford}^{CH_4}$	$n_{1ford}^{O_2}$	E_{a1}
$2,0E15$	$0,9$	$1,1$	35000
A_2	$n_{2ford}^{CO_2}$		E_{a2}
$8,1104E10$	$1,0$		77194
A_3	n_{3ford}^{CO}	$n_{3ford}^{O_2}$	E_{a3}
$2,0E9$	$1,0$	$0,5$	12000

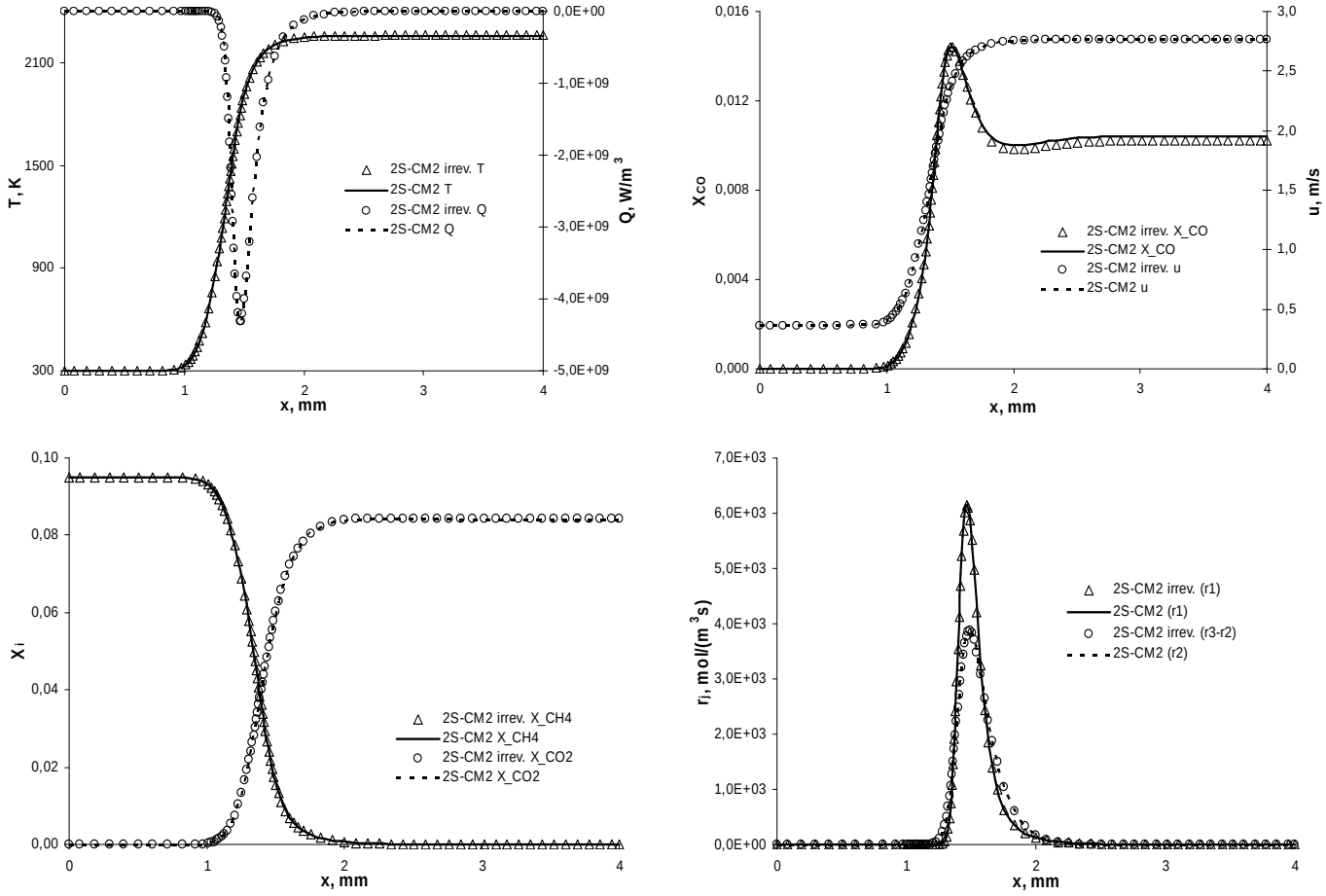

Figure 3: Profiles comparison of 2S-CM2 and irreversible 2S-CM2.

CH_4/AIR FLAMES

Equilibrium computations

Equilibrium calculations of methane oxidation using different reduced mechanisms (various numbers of species) deliver important information about composition and temperature levels, for an adiabatic process. An equilibrium occurs when the forward and the backward reaction rates are equal [28]:

$$k_f \prod_i^N C_i^{\nu_i'} = k_b \prod_i^N C_i^{\nu_i''} \tag{19}$$

where C_i is the i^{th} species concentration according to Eq. (5), ν_i is a molar stoichiometric reaction coefficient, $'$ and $''$ apply for reactants and products respectively.

Mole fractions of species remain stable, because their production rate is equal to their destruction speed. Equilibrium species concentrations do not depend on kinetics, but only on the initial reactant concentration and thermodynamic parameters. The equilibrium constant K_c can be expressed as a relation between forward and backward reaction constants (k_f, k_b) according to Eq. (20) [28].

$$K_c = \frac{k_f}{k_b} = \frac{\prod_i^N C_i^{\nu_i''}}{\prod_i^N C_i^{\nu_i'}} \tag{20}$$

Trying to limit the number of species used to describe a combustion process has a direct effect on the flame temperature (Fig. 4).

Figure 4 indicates, that the adiabatic temperature for the fuel-lean mixture of $CH_4/N_2/O_2$ does not depend strongly on the number of species for the present cases. For near-stoichiometric and fuel-rich conditions the differences are larger, especially for the case with 5 species. This is why the case with five species was not used in further calculations and schemes with at least 6 species were employed (Table 9).

Table 9: Number and kind of species for a conventional combustion of methane in air counting out of argon

Number of species	Species list
52	H_2; H; O; O_2; OH; H_2O; HO_2; H_2O_2; C; CH; CH_2; CH_2(s); CH_3; CH_4; CO; CO_2; HCO; CH_2O; CH_2OH; CH_3O; CH_3OH; C_2H; C_2H_2; C_2H_3; C_2H_4; C_2H_5; C_2H_6; HCCO; CH_2CO; HCCOH; C_3H_7; C_3H_8; CH_2CHO; CH_3CHO; N; NH; NH_2; NH_3; NNH; NO; NO_2; N_2O; HNO; CN; HCN; H_2CN; HCNN; HCNO; HOCN; HNCO; NCO; N_2
7	H_2; O_2; H_2O; CH_4; CO; CO_2; N_2
6	O_2; H_2O; CH_4; CO; CO_2; N_2
5	O_2; H_2O; CH_4; CO_2; N_2

Considering the composition of burned gases, a very good agreement can be observed between the case with 52 and with 7 species for a conventional fuel combustion in air, both for a fuel-rich as well as

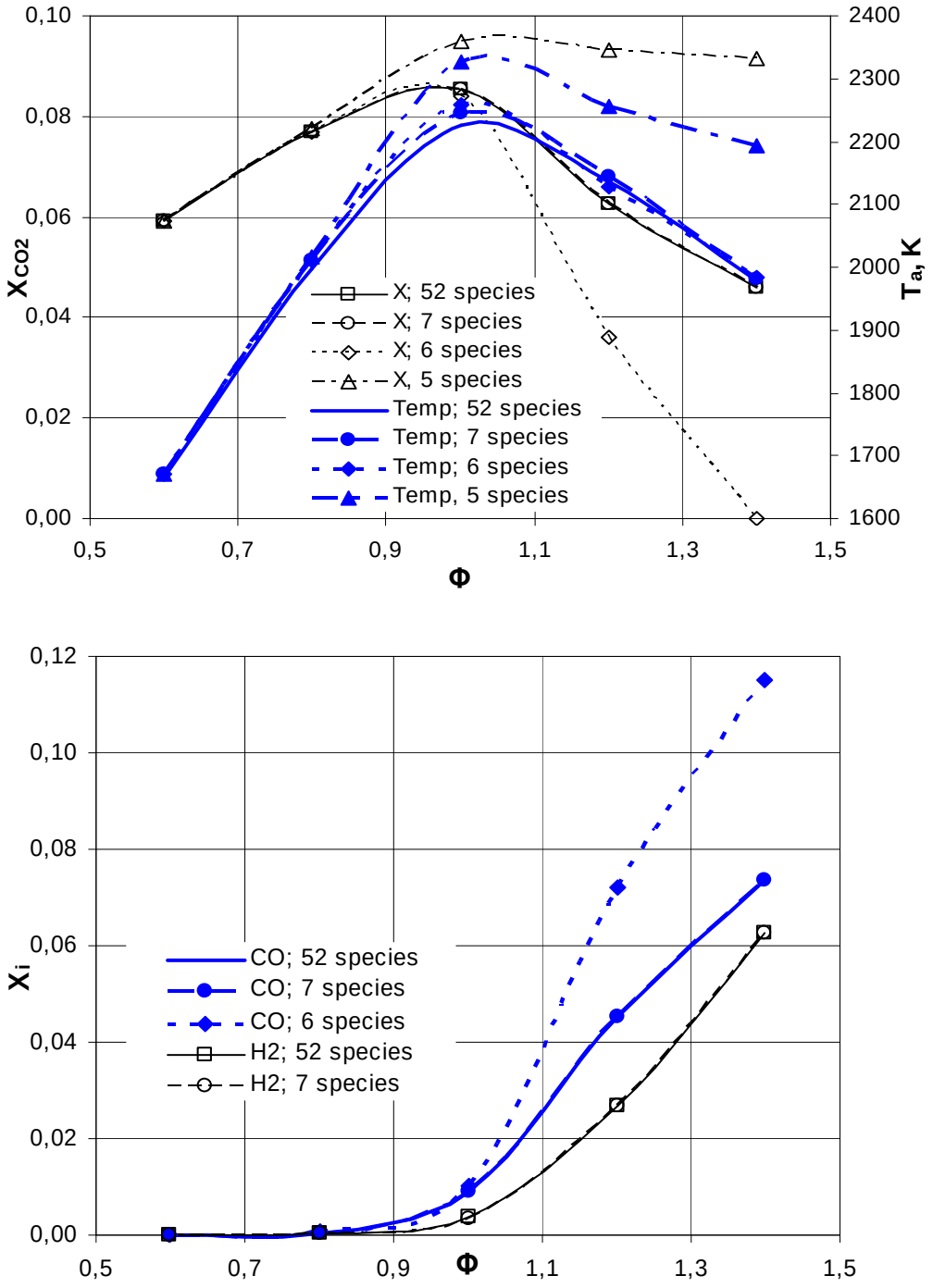

Figure 4: Burned mixture mole fractions and the adiabatic temperature dependence on the equivalence ratio for $CH_4/N_2/O_2$ flame with different oxidation mechanisms for $p_0 = 1bar$, $T_0 = 300K$.

for fuel-lean mixtures (Fig. 4 - top for CO_2 and bottom for CO and H_2). The disagreement for CO, for a case with 52 and 6 species, for a fuel-rich mixture, can be noticed. In the rich zone, the carbon dioxide dissociates leading to an underestimation of CO_2 and over calculation of CO mole fractions.

Auto-ignition delay times

Ignition delays are kinetically controlled substantially, thus they can be used to validate oxidation mechanisms. In Cosilab auto-ignition time delay is defined as a period between completion of the mixing and the "thermal runway", when a maximum temperature, pressure or volume gradient occurs [1]. In this work, a time delay was calculated from the maximum temperature gradient, nevertheless, values obtained from computations from a maximum gradient of volume were almost identical, especially for lower initial temperatures.

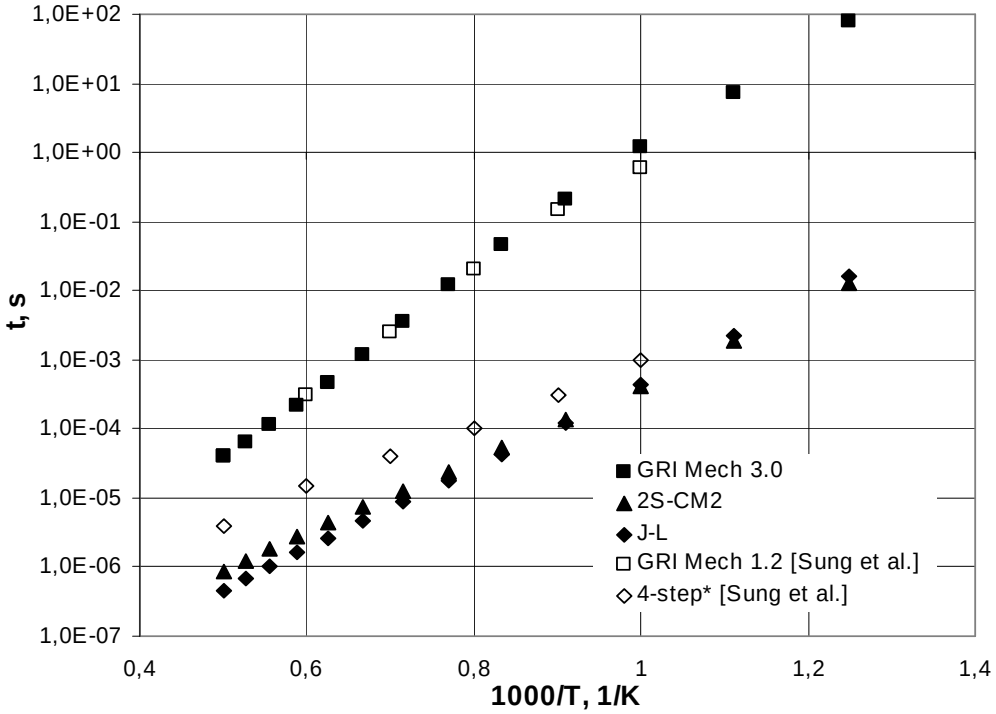

Figure 5: Auto-ignition delay times for $CH_4/N_2/O_2$ mixture, for different oxidations mechanisms, plotted against reciprocal of the initial temperature multiplied by one thousand; filled marks - present work, blank marks - work of Sung et al. [8]; $p_0 = 1bar$, $\phi = 1$.
* 4-step scheme represents mechanism described in the work of Peters and Kee [22], with seven reactants (O_2; H_2O; CH_4; CO; CO_2; H_2 and H).

Figure 5 presents results of auto-ignition delay times, which are plotted against reciprocal of the initial mixture temperature multiplied by one thousand. A significant decrease of auto-ignition delay time with increase of initial temperature was found, for each mechanism. A strong discrepancy is obtained between detailed mechanism calculations using the GRI Mech and the J-L or the 2S-CM2 scheme, nevertheless, the ignition simulations for a present work are in agreement with obtained for GRI Mech 1.2 by Sung et al. [8]. Auto-ignition delay times for a reduced mechanisms (J-L and 2S-CM2) are approximately hundred times shorter than the reference calculations with GRI Mech. A significant disagreement between detailed mechanism and 4-step mechanism was also acquired by Sung et al. [8] (Fig. 5). A good agreement within auto-ignition delay times between detailed mechanism and reduced one was found by researchers when the reduced mechanism consists at least ten reactions [31, 8]. A general conclusion can be drown that highly restrictive 2-step or 4-step reduced schemes are unable to predict the ignition phenomena.

One-dimensional premixed laminar flames

Freely propagating flames are found far enough from combustion chamber walls or from burner nozzles that the disturbance of the flow is not present. This kind of flame can be laminar or turbulent. Multiple methods exist to measure or calculate the laminar flame speed: the propagating flame in a tube, the stagnation point flame, the Bunsen burner and the spherical unsteady flame [18]. In Cosilab it is possible to calculate freely propagating laminar one-dimensional flames (1DFPLF), which in industry rarely exist. However some quantities which are calculated thanks to 1DFPLF can be used for better understanding and advanced modeling of the combustion phenomena (flamelet turbulent model [24, 9]) in real applications.
According to the thermal theory, a mathematical model of the laminar flame contains a few assumptions [17]:

- Heat, which is ensued due to an exothermic oxidation reaction, is transported thanks to conduction (no Dufour effect);
- Mass and heat transfer does not appear between particular stream layers;
- The laminar flame thickness is relatively thin in comparison to the mean free path of a specie.

Because of the low thickness of the high-speed reaction zone, gradients of a temperature and species are large (Fig. 7): the combustion process is self-sustainable due to species diffusion and heat transfer from the reaction zone to the unburned mixture.
During the combustion of a homogenous mixture, the speed of the flame front, in a normal direction to the surface of this flame front, is named the laminar flame speed [21]. According to Eq. (21) the laminar flame speed depends on the square root of diffusion coefficient and reaction rate coefficient [23].

$$s_L \propto (D_{th} \cdot R_r)^{0,5} \tag{21}$$

Determining laminar flame speeds of methane-air mixtures, for various equivalence ratios, can be done experimentally or numerically [18, 3, 12, 29]. Figure 6 presents a comparison of results from works mentioned above and of present calculations using the Cosilab software with the GRI Mech 3.0. The tendencies as well as the values for different researchers are similar. The laminar flame speed attains a maximum value for slightly fuel-rich mixture at equivalence ratio approximately $1,05$ and achieves value circa $0,37 m/s$.

CH_4-N_2-O_2 flames were investigated numerically using 1DFPLF case in the Cosilab. The composition of the oxidizer was chosen to imitate the air in a simple way, thus the mole fractions of O_2 and N_2 were equal respectively to $0,21$ and $0,79$.
Two different simplified chemical kinetics mechanisms were investigated in details to examine their influence on the flame behavior during various parameter alterations. The first one was the two-step oxidation mechanism (2S-CM2) [6] with five reactants (O_2, CH_4, CO_2, H_2O, CO) and N_2 as an inert substance. The second mechanism is Jones-Lindstedt (J-L) [16] four step mechanism with six species which participate in reactions, where the additional specie compared to the 2S-CM2 mechanism is H_2. Results using those two reduced mechanisms were compared to GRI Mech computations. The full specification of the reactions parameters of reduced mechanisms is presented in Tables 3, 5 and 6.

Mole fractions and temperature profiles differ for various mechanisms (Fig. 7), however for the J-L mechanism better agreement can be observed compared to the 2S-CM2 mechanism, particularly for the peak of CO. Carbon monoxide profiles for the two-step and the GRI mechanisms do not overlap; carbon monoxide concentration is under predicted in comparison to the GRI Mech. The J-L mechanism predicts this more precisely; however, the peak of CO is slightly overestimated . While for the four and for the two-step mechanisms of CH_4 oxidation the equilibrium is achieved quite fast, for the detailed mechanism is not reached at all. The temperature and species mole fractions have still gradients in the post-combustion region (Fig. 7). To reach equilibrium the calculated domain has to be extended considerably. Calculated equilibrium species concentrations and the adiabatic temperature have been discussed in the previous chapter of this report; the major topic in this section is chemical kinetics.

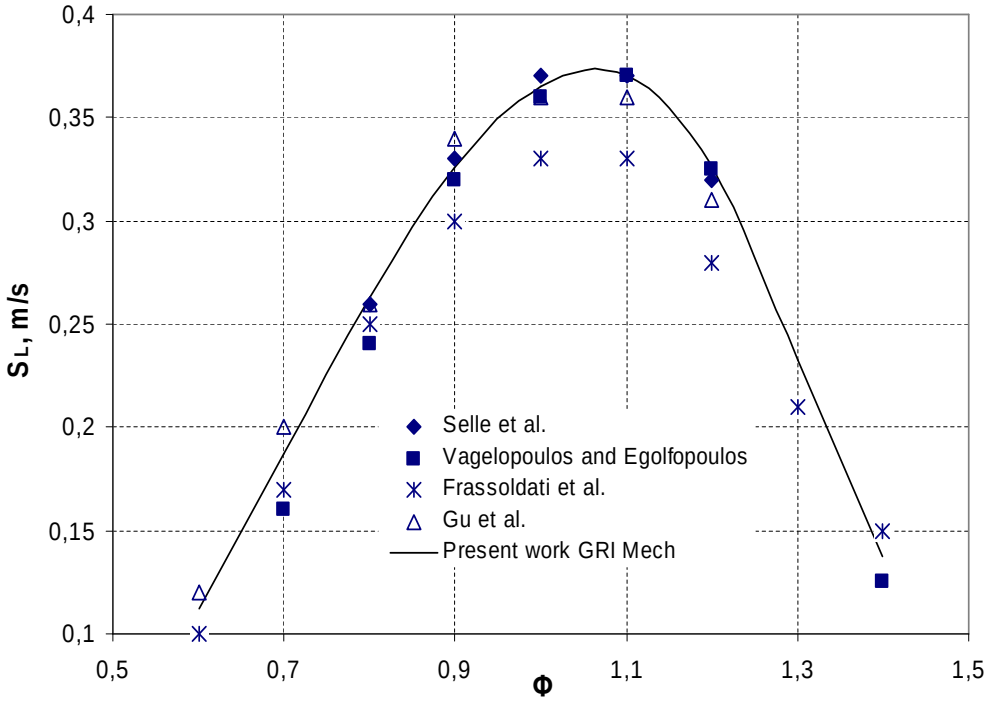

Figure 6: Laminar burning velocities obtained by various workers plotted against equivalence ratio for $p_0 = 1bar$ and $T_0 = 300K$.

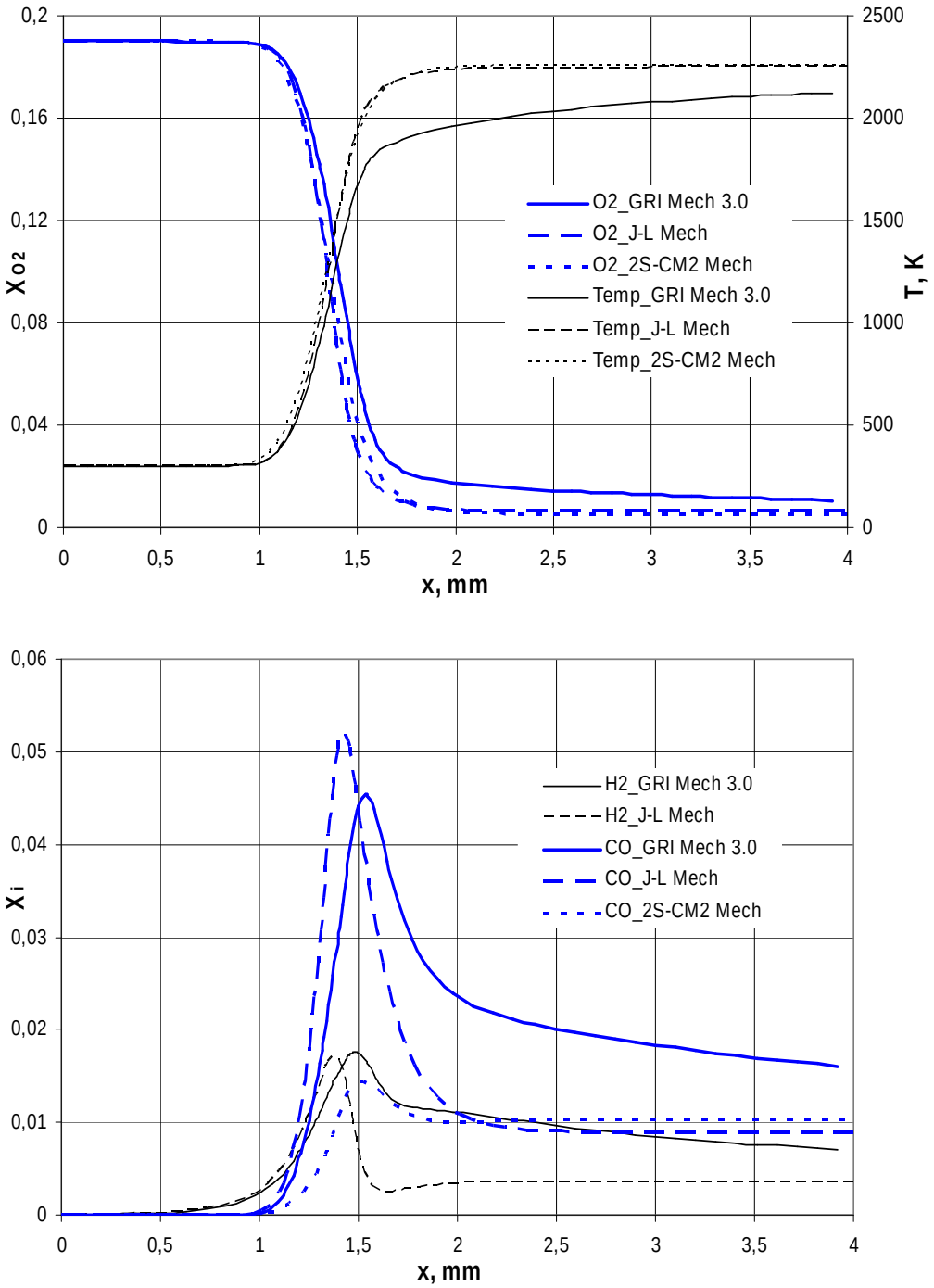

Figure 7: Species and temperature profiles for $CH_4/N_2/O_2$ flame with different oxidation mechanisms for $p_0 = 1bar$, $T_0 = 300K$, $\Phi = 1$.

The capacity of reduced schemes to predict flame speeds for various equivalence ratios is tested in Fig. 8: a systematic overestimation by $0,045 m/s$ for the J-L mechanism, for fuel-lean and nearly stoichiometric flames, can be observed in comparison with the GRI Mech calculations. When the two-step mechanism is employed to calculate the laminar flame speed, for fuel-lean conditions, the accuracy is good. Nevertheless, S_L for fuel-rich conditions is seriously overestimated comparing with GRI Mech. Even the curve tendency does not preserve a proper shape and it is necessary to employ the pre-exponential factor adjustment (PEA) for fuel-rich conditions, in order to cover the full scheme data (chapter - Chemical kinetics). The 2-step mechanism, which utilizes PEA, is 2S-CM2-JB1. A good agreement between outcomes for the detailed mechanism and 2S-CM2-JB1 is found.

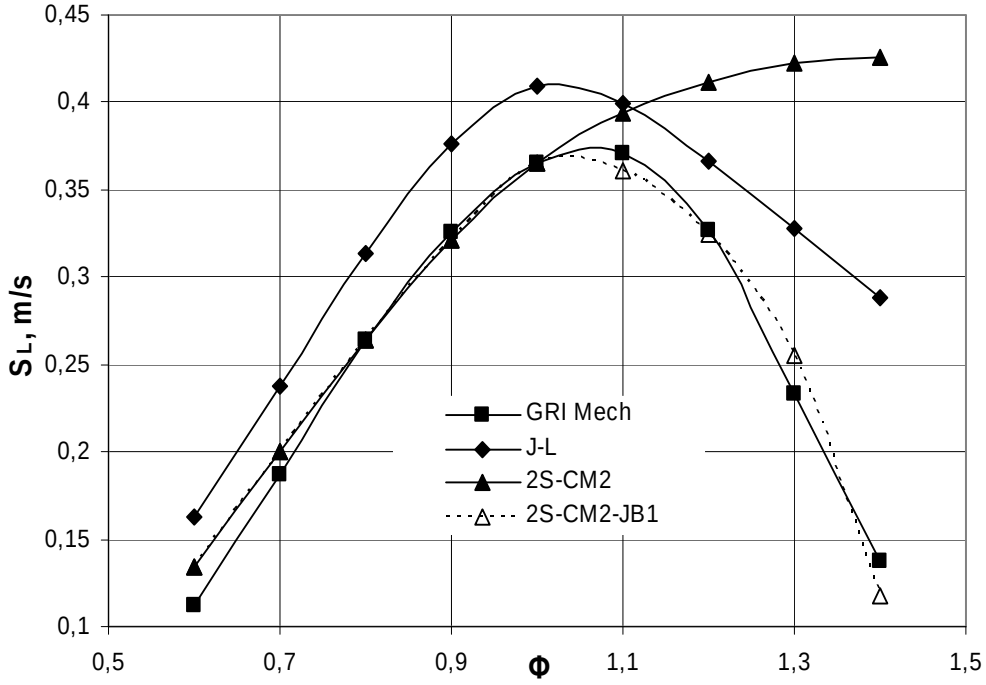

Figure 8: $CH_4/N_2/O_2$ laminar flame speed against equivalence ratio for four different mechanisms; $p_0 = 1 bar$, $T_0 = 300 K$.

One-dimensional stretched premixed laminar flames

The simulation of one-dimensional stretched premixed laminar flames was performed in order to examine reduced schemes in the conditions, which may occur in real applications. In general, counterflow flames are generated by directing two jets towards each other that a stagnation plane or point ($x = 0$), between two identical flames, occur [1] (Fig. 9).

The computational time is saved when only one jet is taken into consideration. The second jet can be created as a mirror image of the existing one, where the stagnation plane is a surface of reflection.
Flame stretch can be defined as an elementary change of the flame surface (A) during infinitely short time [23]:

$$\kappa = \frac{1}{A}\frac{dA}{dt} \tag{22}$$

For stationary flames, stretch can be evaluated as [25]:

$$\kappa = -\frac{du}{dx} \tag{23}$$

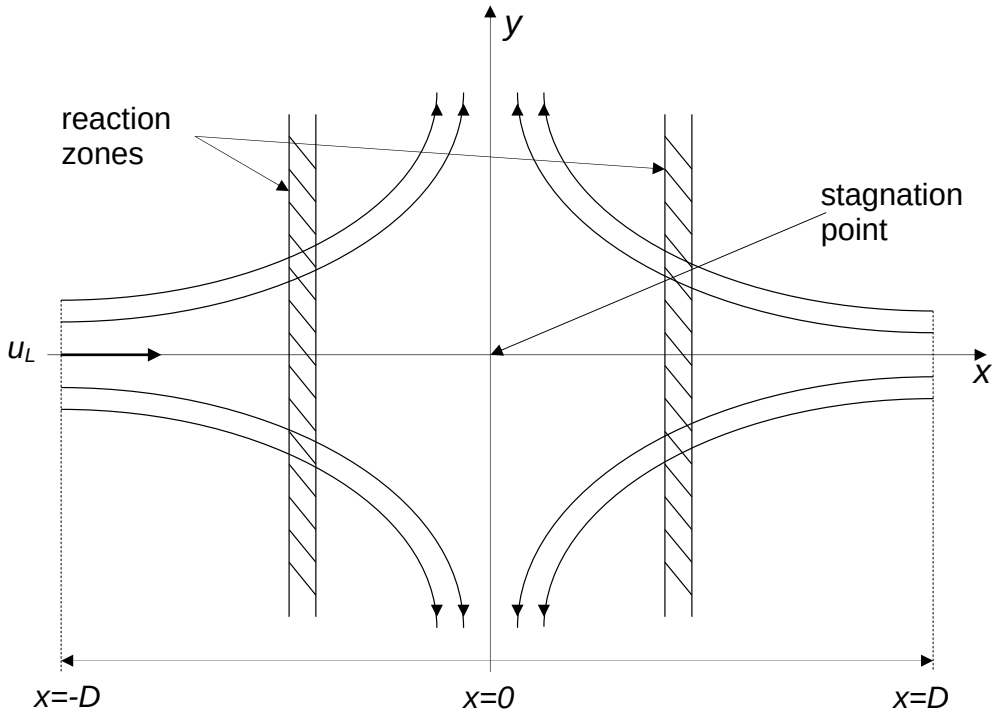

Figure 9: Counterflow premixed flame characterization

where u and x are the mixture velocity in normal direction and the distance from the inlet surface respectively.

Defining stretch rate is difficult [25]. Eq. (22) is local and gives results, which depend on x. This problem was not handled here and instead of κ_L, the velocity u_L was imposed at $x = -D$ to quantify stretch effects. The flame speed response, according to the work of Chao et al. [5], is described with the aid of a minimal flow velocity (u_{min}), which is found at an unburned gas side of the flame, just next to the flame front.

Calculations of premixed stretched methane-air flames were performed for $\phi = 1$, $T_0 = 300K$ and $p_0 = 1bar$. Separation distance (2D) between two jets has an effect on u_min as well as on accuracy of laminar flame speed evaluation [5]. Taking into account the experience of Chao et al. [5], the domain was chosen as big as $20mm$, however, as it was mentioned before, only one half of the domain was calculated. Simulations were performed for different initial mixture velocities ($u_L \in (0,4;2)m/s$), increasing gradually this quantity by $0,2m/s$.

Figure 10 presents profiles of velocity and volumetric heat release (top graph) or temperature and species profiles (bottom graph). A displacement toward fresh mixture, within all profiles, for 2S-CM2 and J-L schemes, can be observed in comparison with profiles obtained for GRI Mech. However, for 2S-CM2 a better agreement was achieved.

Minimum velocities are obtained from velocity profiles. This minimum is reached on the unburned mixture side, just before the flame front (Fig. 10 top graph). Moving towards the stagnation plane, the expansion of the mixture, due to intensive temperature escalation in the flame front, accelerates the mixture. Crossing the zone, where intensive heat release occurs, the velocity starts to decrease and the speed, in the normal direction to the inlet surface, reaches value equal to 0 at the stagnation point. Due to a more intense heat release, the velocity for the J-L mechanism reaches the highest value in the flame front.

Carbon monoxide peaks reach similar values for GRI Mech and J-L schemes (Fig. 10 bottom graph), nevertheless, for the GRI Mech mechanism, the concentration of species does not reach the equilibrium, as observed in the freely propagating flame (Fig. 7). Peak of CO for 2-step mechanism (2S-CM2) is

underestimated highly.

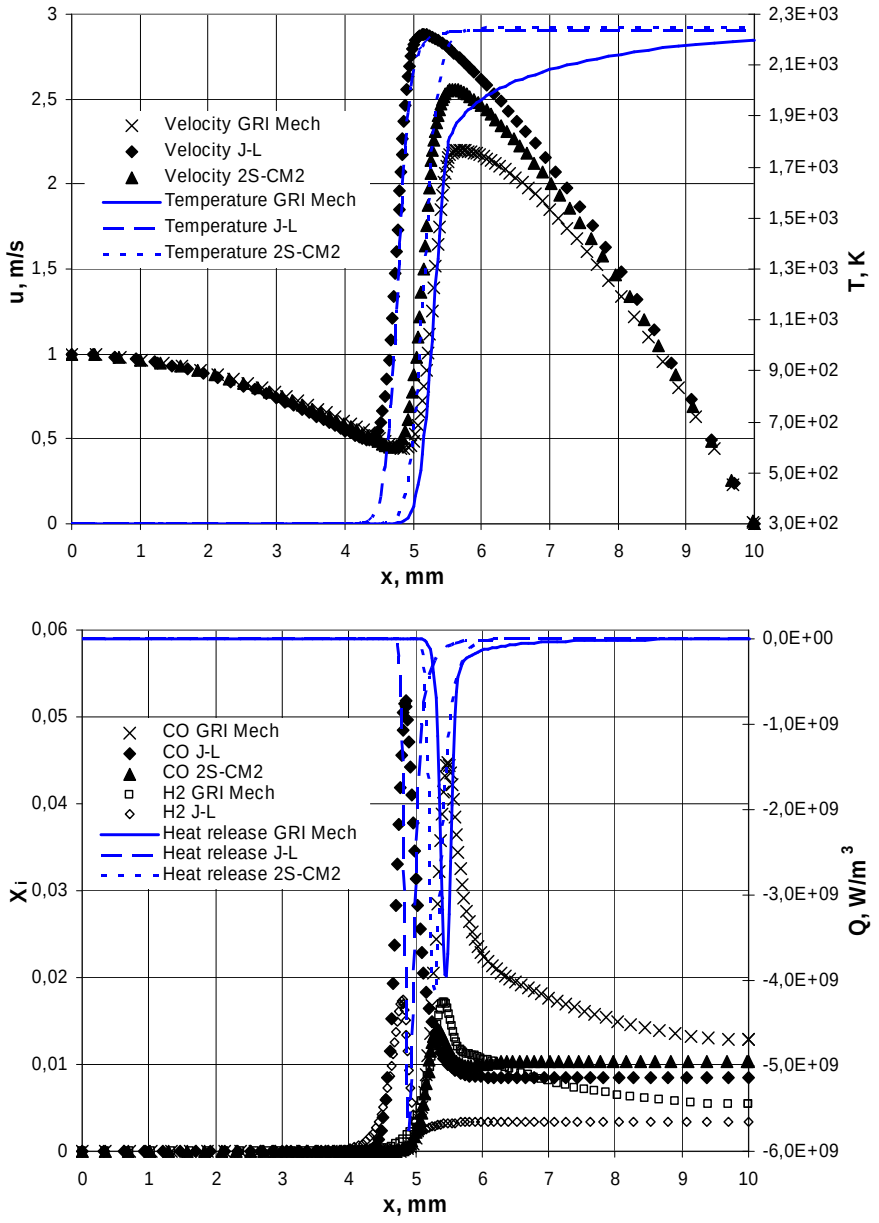

Figure 10: Species, temperature, velocity and heat release profiles for $CH_4/N_2/O_2$ flames for different mechanisms for $p_0 = 1bar$, $T_0 = 300K$, $\Phi = 1$, $u_L = 1m/s$.

Minimum mixture velocity against inlet velocity is plotted in figure 11. A good agreement for the 2S-CM2 and the GRI Mech schemes can be found, while the J-L mechanisms overestimates the u_{min} quite considerably. A better agreement was achieved for lower values of the inlet mixture velocity for both the 2S-CM2 and the J-L schemes with the detailed chemistry simulation. A nearly linear behavior of u_{min} with u_L was obtained for larger values of inlet mixture speed ($u_L > 0,8m/s$). Nevertheless, while further decrease of the inlet velocity nearby the value obtained for freely propagating flame simulation (S_L), the linear tendency is lost. The strongly nonlinear behavior is found, which is in agreement with results obtained by Chao et al. [5]. When the inlet mixture velocity reaches values close to the laminar flame speed ($u_L = u_{min}$) the flame is unstretched ($\kappa = 0$).

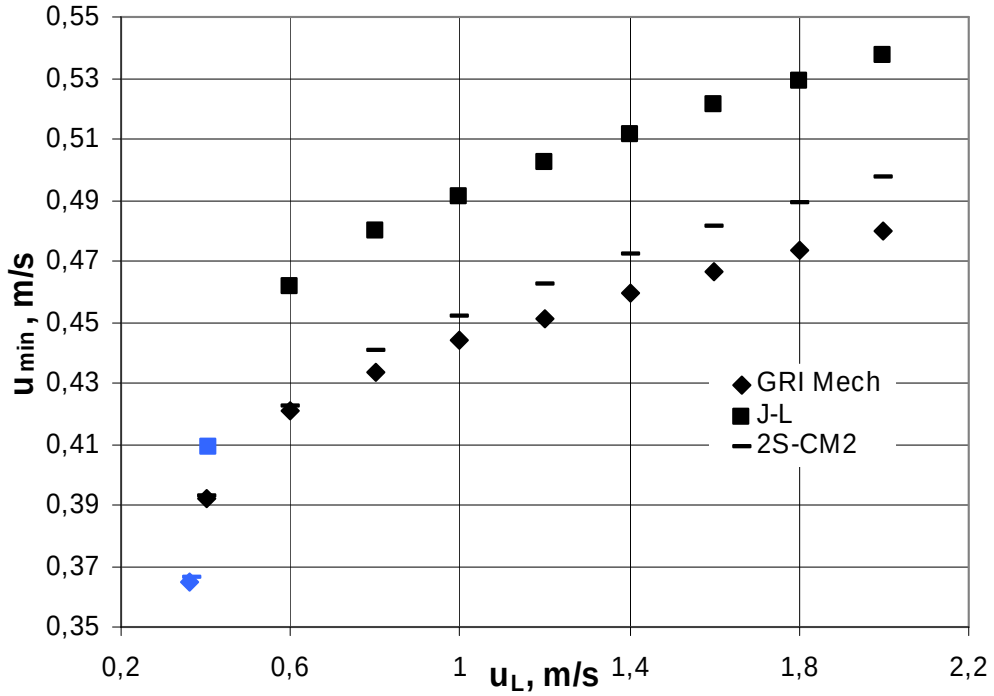

Figure 11: Minimum mixture velocity plotted against inlet velocity for $CH_4/N_2/O_2$ flames for different mechanisms for $p_0 = 1bar$, $T_0 = 300K$, $\Phi = 1$; Brightened marks for $u_L = u_{min}$ are calculated using 1D simulation of freely propagating laminar flame.

One-dimensional stretched diffusion laminar flames

In this section, the laminar stretched diffusion flames will be considered. This kind of flame is formed when fuel and oxidizer are not mixed before they enter to the combustion chamber. Counterflow flames are created when two jet streams are directed opposed to each other, what regarding diffusion flame, means that one jet constitutes only fuel, one only oxidizer. A fuel and an oxidizer diffuse towards the reaction zone, where rapid oxidation reactions take place and thus heat is generated. The most reactive region of diffusion flames is situated at local stoichiometric conditions for a mixture fraction equal to [20]:

$$z_{st} = \frac{1}{1+\phi_b} \tag{24}$$

where ϕ_b is characterized by Equation (9).

On the fuel side of the flame (in this work - left) and on the oxidizer side (right), the mixture is too rich or too lean to burn, therefore, the flame does not propagate toward inlets. This is the main advantage of the diffusion flame in term of safety. However, because of the time required for reactants mixing, inside the combustion chamber, the burning efficiency is suppressed in comparison to premixed flames.

The simulations were performed for the detailed mechanism and for the 2S-CM2 scheme. For computations with the J-L mechanism problems with convergence were found. The reason for this problem could be a negative order for one of the reversible reaction (Table 6). The domain, which was used for diffusion flame calculations, was as large as $10mm$. Various strain rate values were tested in the range of $1-250$. The strain rate, in comparison with premixed counterflow flames, was one of input parameters.

Figure 12 presents profiles of the velocity and of the heat release obtained for the detailed chemistry and the 2S-CM2 scheme, for a strain rate $\kappa = 100$. The top graph presents result for unchanged coordinates for the 2-step mechanism, while the bottom graph shows those two quantities, where coordinates for the 2S-CM2 were shifted towards profiles for the GRI Mech. A good agreement in terms of velocity profiles were found, between those two mechanisms.

The observed flame displacement, for the 2-step mechanism in comparison with the GRI Mech, was probably caused by not complete problem convergence, however a shifting of the flame did not have influence on profiles character. The second reason for this behavior could have source in the difference, within the integrated fuel reaction rate ($\dot{\Omega}_F$), for the 2-step mechanism and the GRI Mech. The integrated fuel reaction rate per unit flame area was calculated according to equation below [23]:

$$\dot{\Omega}_F = \int_{x_f^-}^{x_f^+} \dot{\omega}_F dx$$

where $\dot{\omega}_F$ is the fuel rate of destruction in $mol/(m^3 \cdot s)$; x_f^- and x_f^+ are points located infinitely close to the flame front on both side of it.

The absolute value of this quantity was always larger, when the detailed mechanism was employed in the calculations (Figure 13). However, the difference of $\dot{\Omega}_F$, between the 2-step mechanism and the GRI Mech, was not so significant for lower strain rates as it was obtained for higher values of this quantity.

A very good agreement was found for some of the main species (H_2, O_2 and CH_4) profiles between the 2S-CM2 and the GRI Mech (Figure 14). Nevertheless, a significant difference between CO, CO_2 mole fractions and temperature profiles was found. An insufficient CO_2 decomposition to carbon monoxide could cause the escalation of the temperature for the 2S-CM2 mechanism in comparison with the GRI Mech.

A flame shifting towards the fuel inlet was observed, when the strain rate was increased for detailed chemistry calculations (Figure 15). A higher stretch invoked the flame to be more compact and caused that the temperature gradients were larger.

In results postprocessing, of the diffusion flame, it is very common to plot graphs of different quantities against a mixture fraction (z), which indicate the ratio between a fuel and an oxidizer. The detailed

mechanism, which was used in simulation of diffusion flames, requires that the mixture fraction will be calculated with respect of radicals. It was done according to Equation (11). Figure 16 presents results of species mass fraction and temperature plotted against the mixture fraction based on atoms. The dependence of oxygen and fuel mass fractions with the mixture fraction preserves the correct behavior described in the literature [23]. Almost linear tendency was found for all major species, where the point of bend for those curves lays next to the stoichiometric mixture fraction (z_{st}) defined according to Equation (24).

Figure 17 shows a good agreement between results obtained for the GRI Mech, the 2S-CM2 and equilibrium calculations, for the mixture fraction lower than a stoichiometric value of this quantity ($z_c < z_{st}$), thus for a fuel-lean side of the flame. Nevertheless, for $z_c > z_{st}$ the difference, between those computations, becomes significant. Higher temperatures, in comparison with equilibrium calculations, for a fuel-rich side of the flame, for both the GRI Mech and the 2S-CM2, were obtained (fig. 35). This temperature is called "super-equilibrium temperature" and according to available literature [20, 15, 27], can be explained by differences in species diffusivities and heat transport, when detailed full transport species data is employed in calculations.

A maximum temperature in diffusion flames is an important quantity. In general, the maximum temperature is obtained for stoichiometric value of the mixture fraction, where exothermic reactions progress relatively fast, in comparison to other regions of the flame. The maximum temperature is decreasing with increasing the strain rate for higher values of this quantity (Figure 19). Further increase of the strain rate could cause that the heat flux density, between the burned gases and the fresh mixture, is not sufficient to support the combustion process (quenching point).
For lower strain rates ($\kappa < (30-50)$, the maximum temperature with stretch behaved incorrectly with theory. This was probably the result of too narrow domain that was used in calculations, while the flame became wide, for a lower values of strain rate.

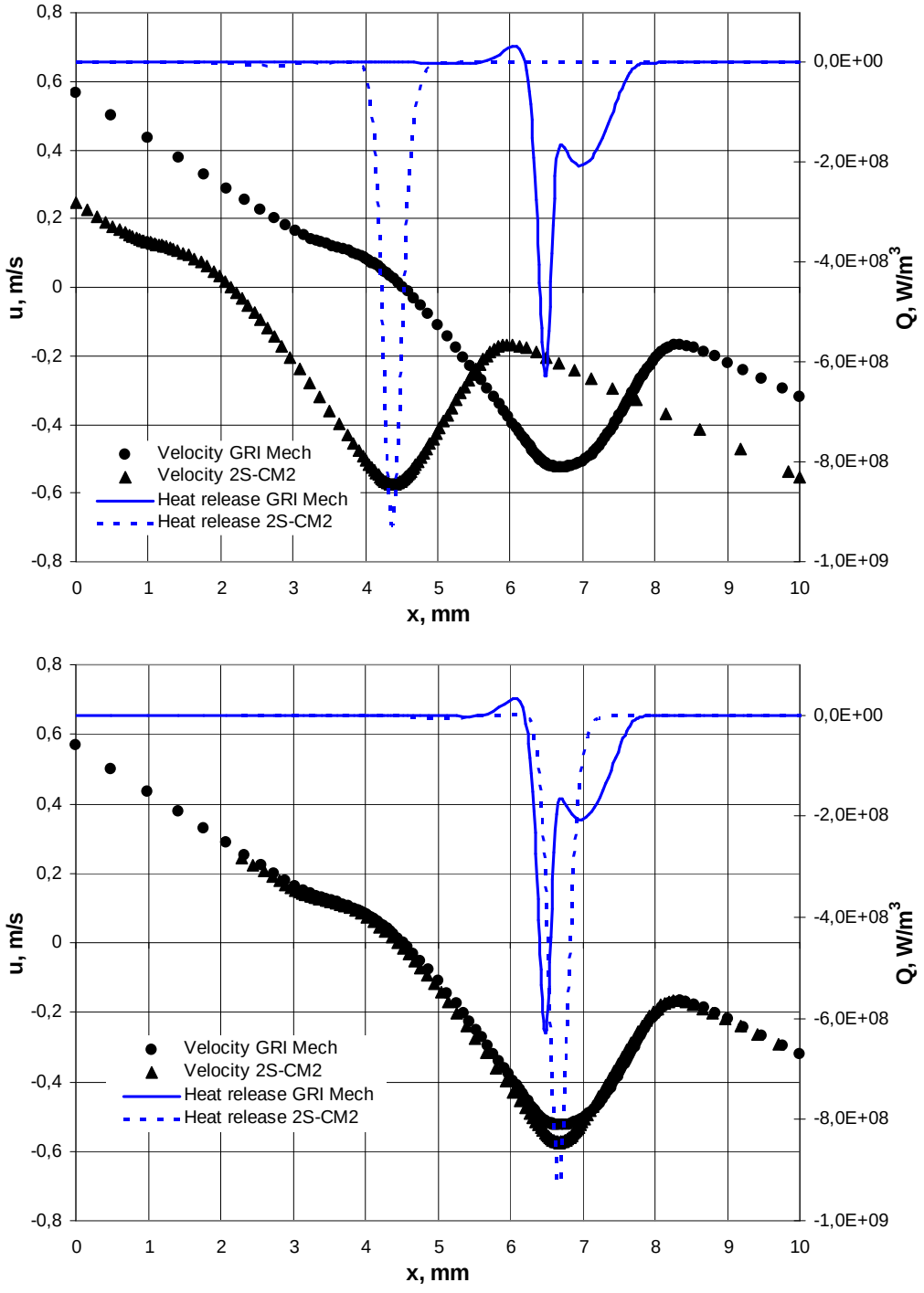

Figure 12: Velocity and heat release profiles comparison for the GRI Mech and the 2S-CM2; $CH_4/N_2/O_2$ diffusion flame; $p_0 = 1bar$, $T_0 = 300K$, $\kappa = 100$.

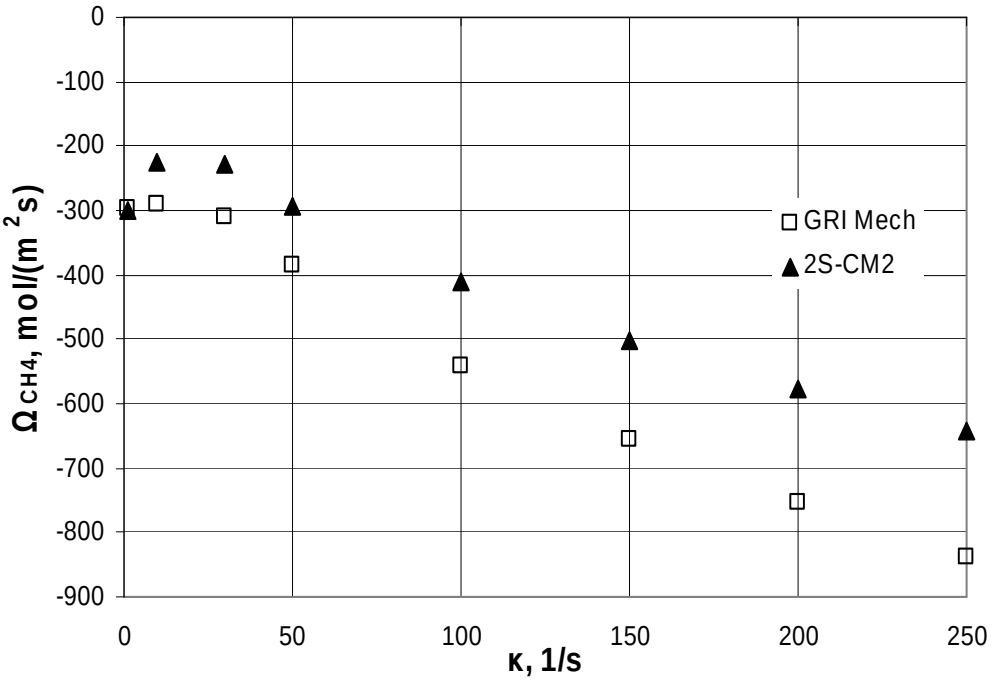

Figure 13: Integrated fuel reaction rates plotted against strain rates for the GRI Mech and the 2S-CM2; $CH_4/N_2/O_2$ diffusion flame; $p_0 = 1bar$, $T_0 = 300K$.

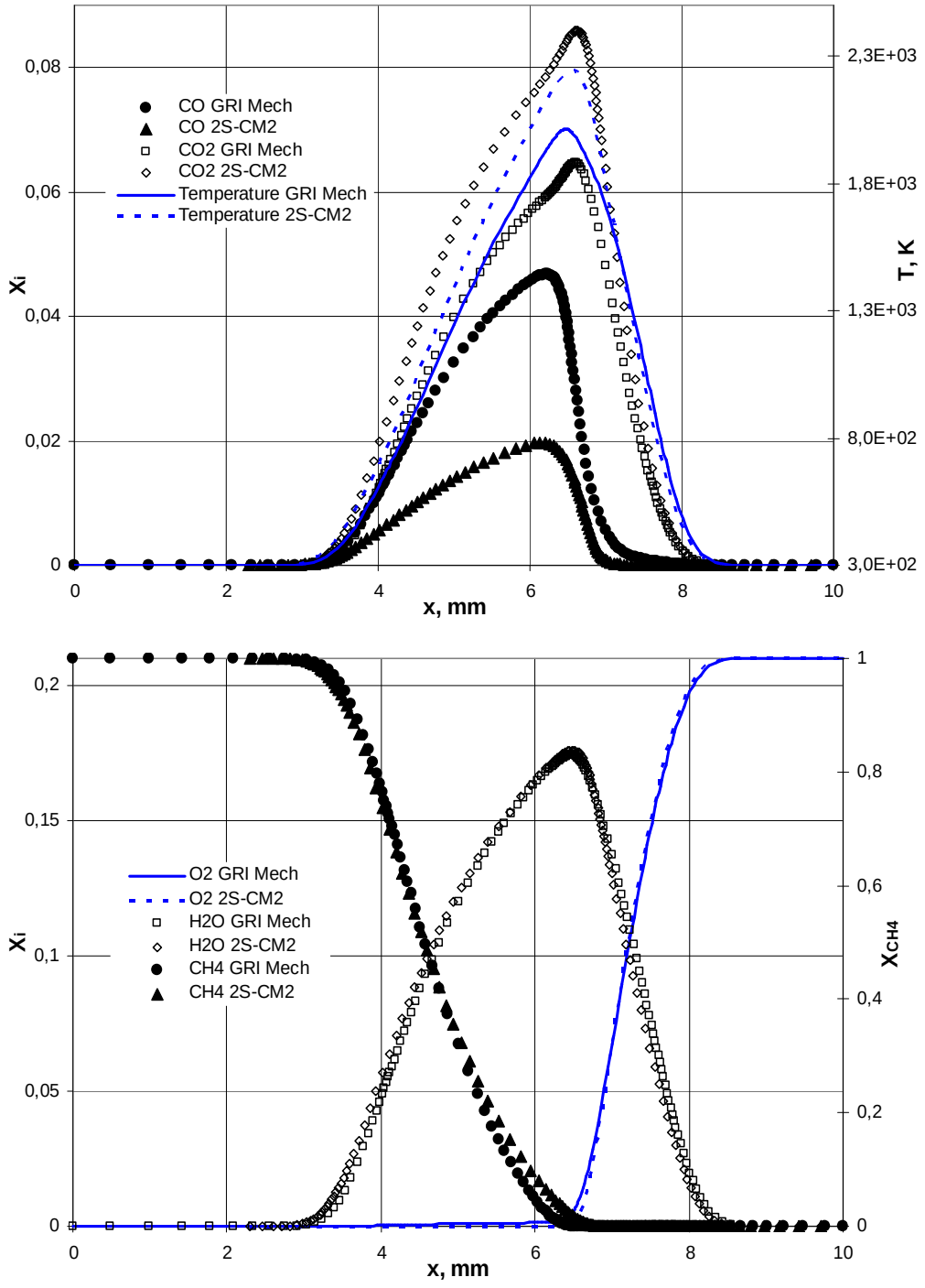

Figure 14: Species and temperature profiles for the GRI Mech and the 2S-CM2; $CH_4/N_2/O_2$ diffusion flame; $p_0 = 1bar$, $T_0 = 300K$, $\kappa = 100$.

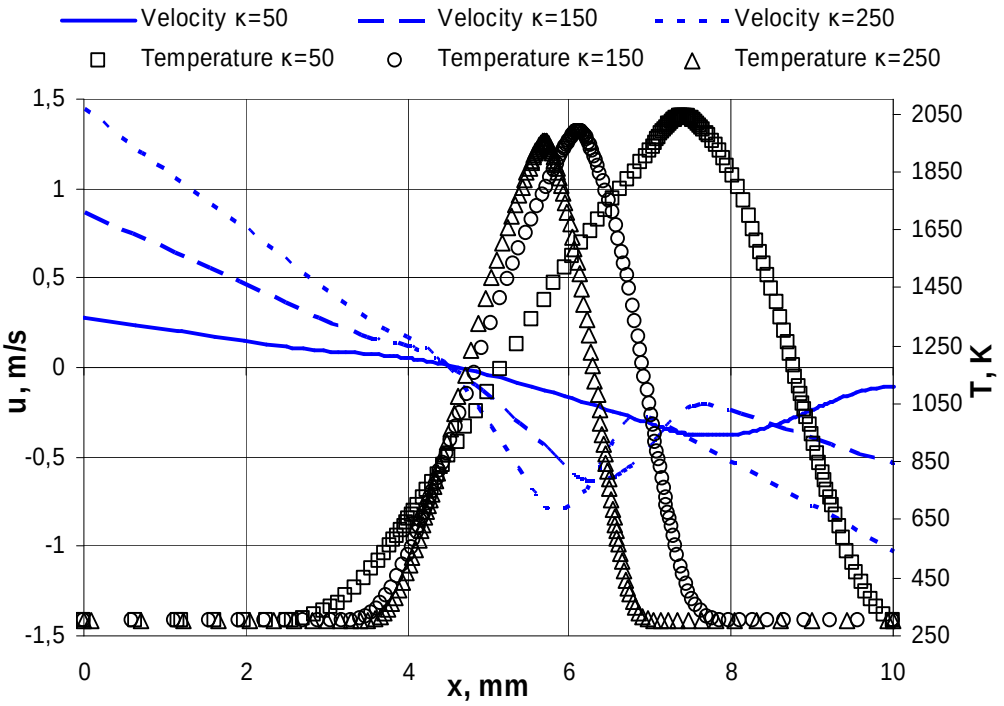

Figure 15: Profiles of the temperature and velocity for various stretch rates; GRI Mech; $CH_4/N_2/O_2$ diffusion flame; $p_0 = 1bar$, $T_0 = 300K$.

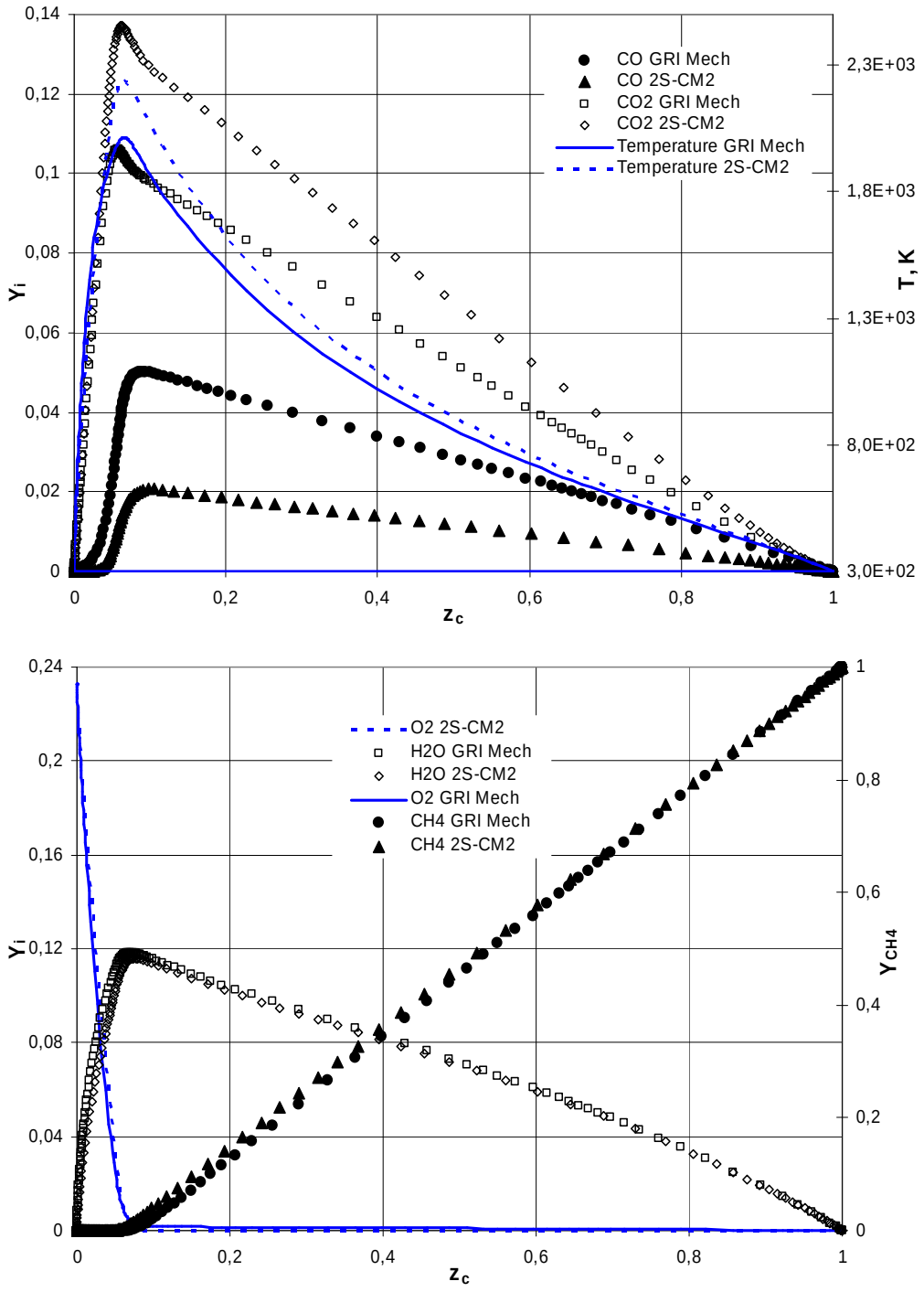

Figure 16: Species mass fractions and temperature plotted against mixture fraction for the GRI Mech and the 2S-CM2; $CH_4/N_2/O_2$ diffusion flame; $p_0 = 1bar$, $T_0 = 300K$, $\kappa = 100$.

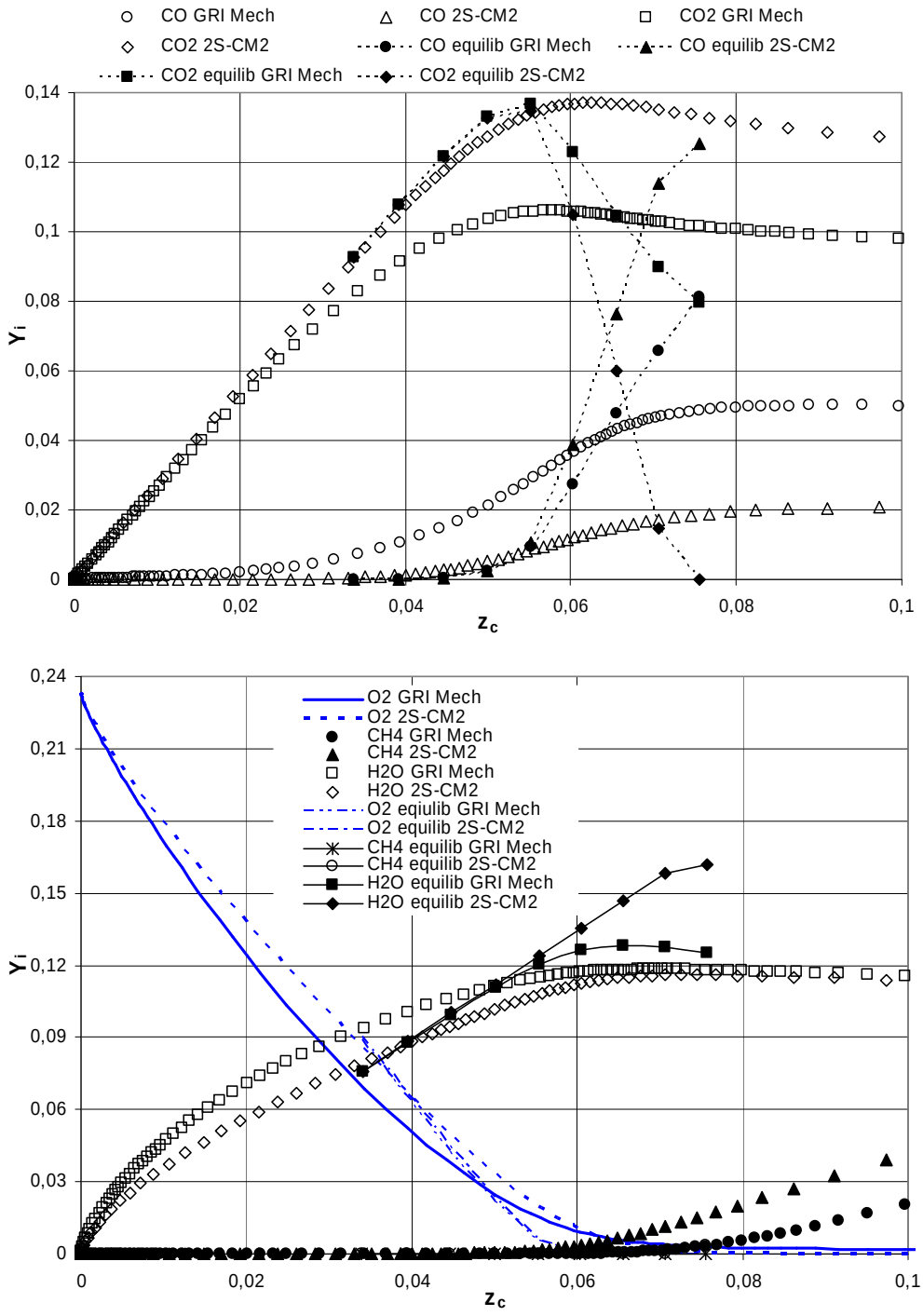

Figure 17: Species mass fractions plotted against mixture fraction for the GRI Mech, the 2S-CM2 and evaluated from equilibrium calculations; $CH_4/N_2/O_2$ diffusion flame; $p_0 = 1bar$, $T_0 = 300K$, $\kappa = 100$.

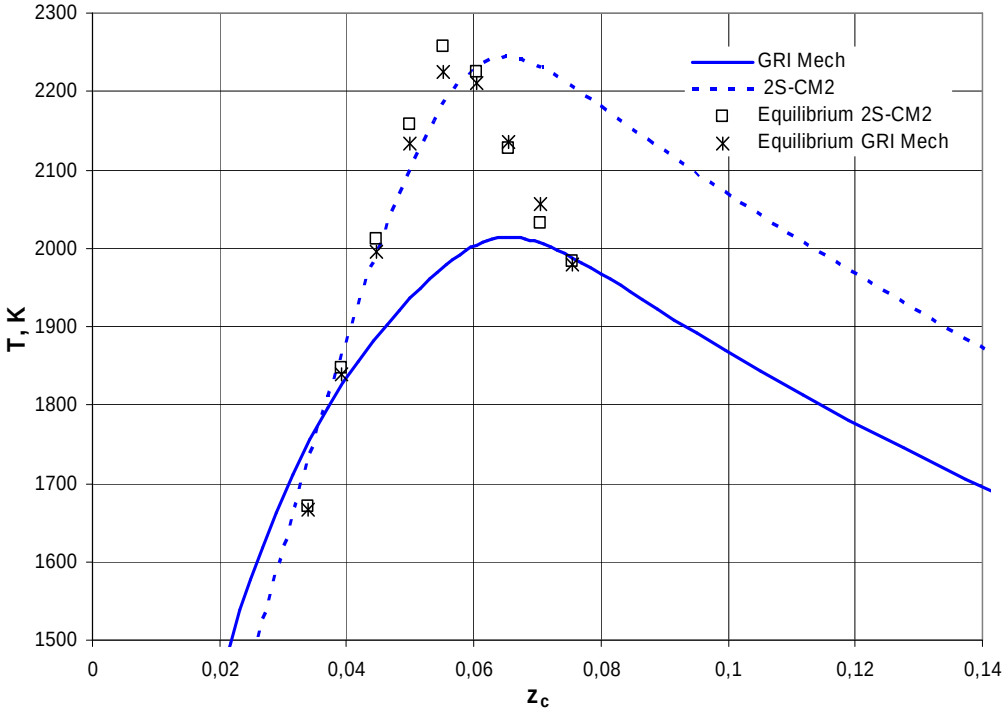

Figure 18: Temperature plotted against mixture fraction for the GRI Mech, the 2S-CM2 and evaluated from equilibrium calculations; $CH_4/N_2/O_2$ diffusion flame; $p_0 = 1bar$, $T_0 = 300K$, $\kappa = 100$.

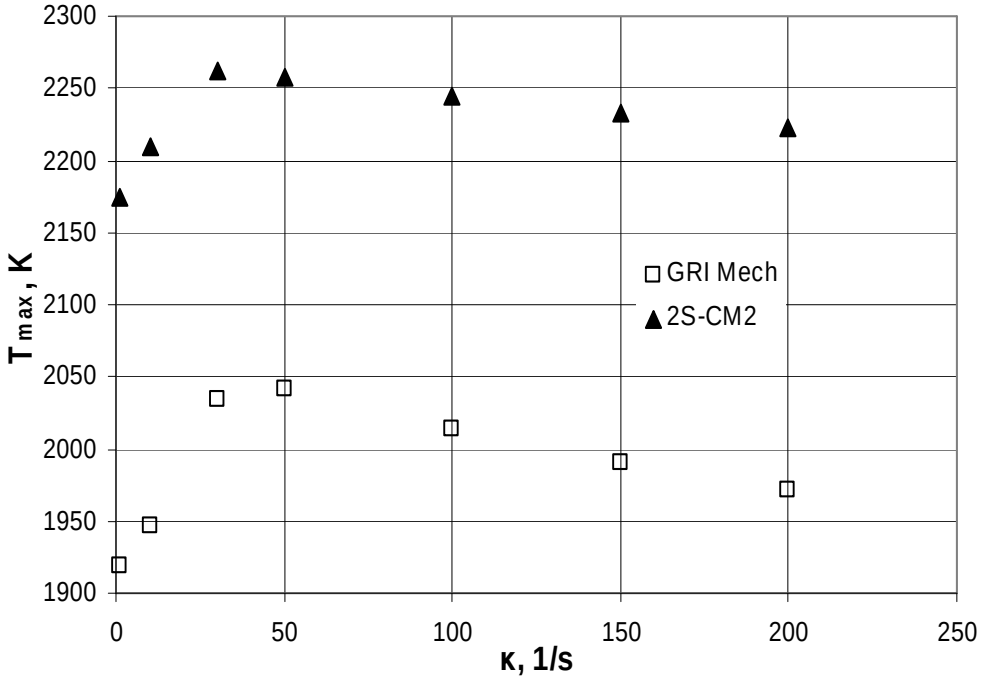

Figure 19: The comparison of the maximum temperature plotted against stretch rate for the GRI Mech and the 2S-CM2; $CH_4/N_2/O_2$ diffusion flame; $p_0 = 1bar$, $T_0 = 300K$.

$CH_4/O_2/CO_2$ FLAMES

Equilibrium computations

The quantity used to measure the CO_2 presence in the oxidizer is $X_{CO_2}^{oxid}$, the mole fraction of carbon dioxide in the oxidizer stream. It is 0 for pure oxygen and was changed up to 70% in this chapter. For higher temperatures, obtained during oxy-fuel conditions with oxygen-rich oxidizer, the difference between calculated adiabatic temperatures for various number of species is much greater than during the conventional combustion in air (Fig. 20). The higher adiabatic temperature difference occurs when less carbon dioxide is present in the oxidizer. The reason is that in higher temperatures oxidation reactions products undergo dissociation and this requires energy. The smallest temperatures are obtained when all 34 species are considered (Table 9). For the case with one-step mechanism, dissociation reactions do not exist, thus the temperature is too high (Fig. 20). The distinction between the adiabatic temperature of the case with 34 species and with 4 species, for pure oxygen-methane flames, is as big as 2100K. Among other reasons, this why the case with four species was not employed for further calculations.

Table 10: Number and kind of species for oxy-fuel combustion of methane

Number of species	Species list
34	H_2; H; O; O_2; OH; H_2O; HO_2; H_2O_2; C; CH; CH_2; CH_2(s); CH_3; CH_4; CO; CO_2; HCO; CH_2O; CH_2OH; CH_3O; CH_3OH; C_2H; C_2H_2; C_2H_3; C_2H_4; C_2H_5; C_2H_6; HCCO; CH_2CO; HCCOH; C_3H_7; C_3H_8; CH_2CHO; CH_3CHO
6	H_2; O_2; H_2O; CH_4; CO; CO_2
5	O_2; H_2O; CH_4; CO; CO_2
4	O_2; H_2O; CH_4; CO_2

The underestimation of CO_2 and over prediction of CO mole fraction for 5 species was found in the oxy-fuel case (Fig. 20). This tendency is intensified for greater mole fractions of molecular oxygen in the oxidizer, thus for larger temperatures. A quite good agreement was found in mole fractions of various species, between the case with 6 and 34 species, in comparison to graphs plotted for less reactants. Nevertheless, the difference is still large especially for larger oxygen fraction in the oxidizer. Regarding the work of Frassoldati et al. [3], at temperatures higher than $2500K$ not only H_2 and CO have significant impacts in limiting the temperature, but also radicals. This suggests that six species will not be enough to describe properly the real flame for the higher oxygen mole fraction ($> 50\%$) in the oxidizer.

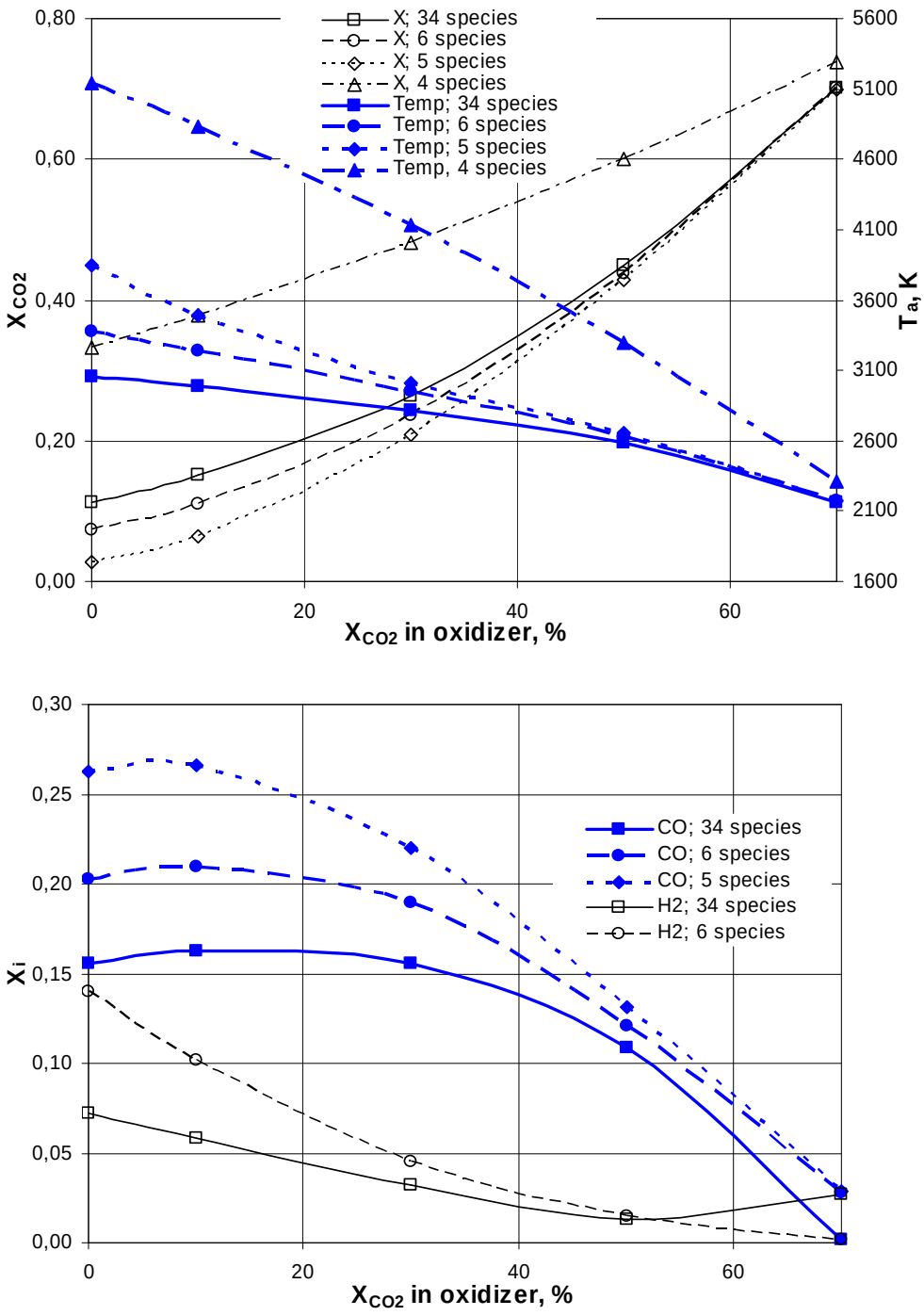

Figure 20: Burned mixture mole fractions and the adiabatic temperature plotted against mole fraction of CO_2 in the oxidizer for $CH_4/CO_2/O_2$ flame with different oxidation mechanisms for $p_0 = 1bar$, $T_0 = 300K$, $\Phi = 1$.

Auto-ignition delay times

Auto-ignition delay times for a mixture, which is composed of methane, molecular oxygen and carbon dioxide are presented in Figure 22. For an oxy-fuel combustion as well as for a conventional combustion of methane in air (Fig. 5) a great disagreement was found between GRI Mech scheme and reduced mechanisms (J-L-JB and 2S-CM2-JB2), which only confirms the argument that low-number reaction schemes are not able to predict the ignition process. The divergence between results obtained for the detailed mechanisms and reduced ones is larger for lower initial temperatures.
Profiles of temperature and volumetric heat release for initial temperature equal to $1500K$ are plotted in Figure 21. A difference between different oxidation mechanisms can be seen clearly. The lowest time delay at the same time with the most intensive heat release is achieved for a case with 2S-CM2-JB2 mechanism. Obviously, the temperature for the detailed mechanism reaches the lowest level, what was explained in details in the chapter that deals with equilibrium calculations.

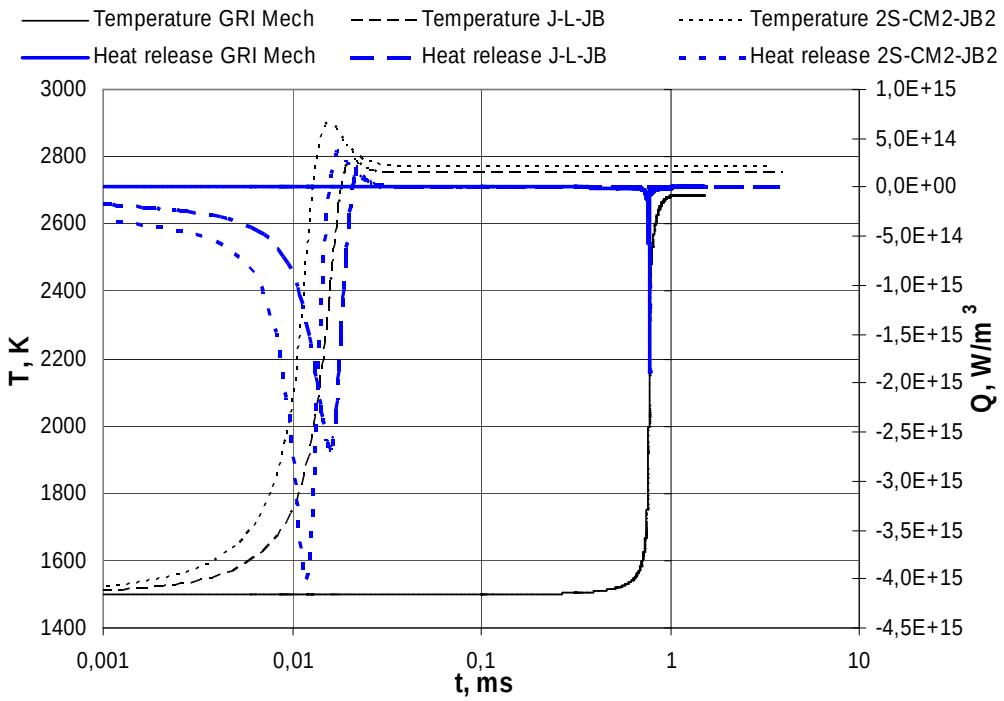

Figure 21: Temperature and volumetric heat release profiles for $CH_4/CO_2/O_2$ mixture, for CO_2=61,5% mole fraction in the oxidizer, for different oxidations mechanisms, plotted against time; $p_0 = 1bar$, T_{init}=1500K, $\phi = 1$.

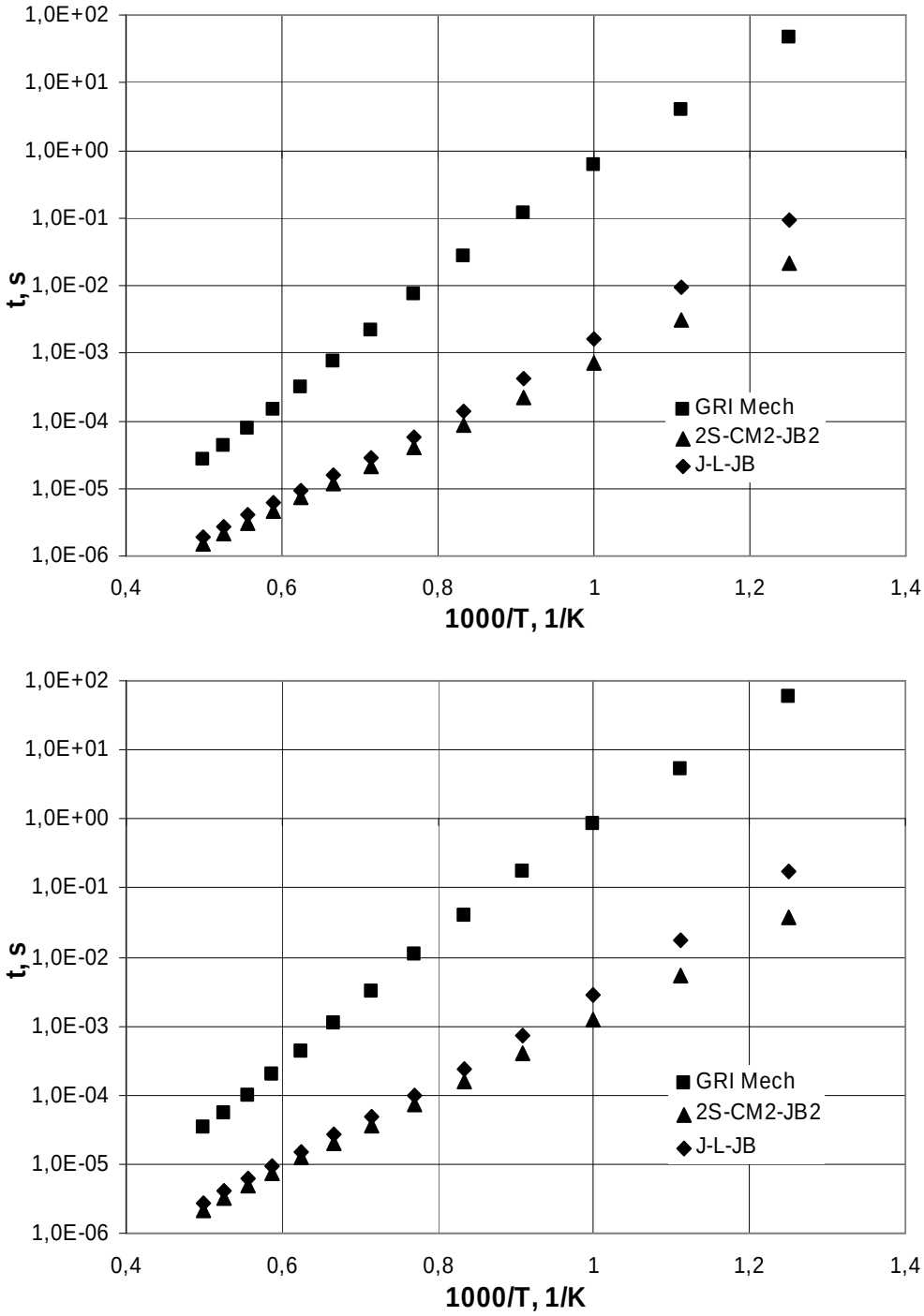

Figure 22: Auto-ignition delay times for $CH_4/CO_2/O_2$ mixture, for CO_2=61,5% (top graph) and CO_2=72% (bottom graph) mole fraction in the oxidizer, for different oxidations mechanisms, plotted against reciprocal of the initial temperature multiplied by one thousand; $p_0 = 1bar$, $\phi = 1$.

One-dimensional premixed laminar flames

The different diffusivity and thermal capacity of carbon dioxide and molecular nitrogen modify the combustion of CH_4. According to the dependency of the laminar flame speed on the diffusion coefficient (Eq. (21)), lower thermal diffusivity in the CO_2 atmosphere influences the laminar flame speed. Different oxidizer compositions have effects on the chemistry itself. The dissociation of CO_2 affects the production of carbon monoxide for higher temperatures (¿1300K) [14]. Nevertheless, a thermal effect on a laminar flame speed decrease was found as the major one by Benedetto et al. [2]. Carbon dioxide has a higher specific heat capacity than N_2, so that the flame has a much lower temperature compared to conventional combustion in air, for the same mole fraction of diluents in the oxidizer. Lower temperatures also have an impact on the combustion rate, which in conjunction with a lower thermal diffusivity and changes in chemistry cause a big difference in laminar flame speed values (Table 11).

Table 11: Summary of laminar flame speed values obtained during present work for methane oxidation simulation in $O_2 = 21\%/N_2 = 79\%$ and $O_2 = 21\%/CO_2 = 79\%$ for various equivalence ratios, for detailed mechanism (in mm/s).

	$\phi = 0,8$	$\phi = 0,9$	$\phi = 1,0$	$\phi = 1,1$
N_2/O_2	0,263	0,326	0,365	0,370
CO_2/O_2	0,026	0,033	0,036	0,033

Calculations for different mole fractions of CO_2 and O_2 in the oxidizer were performed in order to find the laminar flame speed which was obtained during a detailed chemistry simulation of a methane combustion in the environment similar to air. Adiabatic flame temperature and laminar flame speed variations with CO_2 mole fractions in the oxidizer are presented in figure 23. The adiabatic temperature and the laminar flame speed are inversely proportional to the CO_2 mole fraction in the oxidizer. A good agreement between present work and CH_4 combustion simulation in Chemkin-Premix [2] can be observed. For both adiabatic temperature and laminar flame speed, compatibility is much better for higher mole fraction of oxygen in the oxidizer. For pure oxygen-methane flame the temperature reaches value at about 3050K and laminar flame speed is in the order of $3,1 m/s$.

For various equivalence ratio the laminar flame speed tendency is similar to that, which was obtained for N_2/O_2 case. However the maximum value is obtained for slightly fuel-lean conditions, especially for lower O_2 dilution using CO_2 (Fig. 24). General conclusion can be created, that the laminar flame speed is depended strongly on the oxygen concentration in the oxidizer.

Carbon dioxide mole fraction in the oxidizer, for which values of the laminar flame speed is approximately equal to the values obtained during combustion simulation in N_2/O_2 environment, is equal to 0,615, for the equivalence ratio around one (Fig. 25). The further the mixture is from stoichiometric conditions the S_L value disagree more. The adiabatic temperature is elevated for the CO_2/O_2 case at about 250K roughly. Due to a flame stabilization, when an oxidizer is shifted from an air to a mixture of CO_2/O_2, achieving similar laminar flame speeds for an oxy-fuel and a conventional combustion is important.

Figure 26 presents adiabatic temperature results for three different basic oxidation mechanisms described in this report (top graph). Adiabatic temperatures for the J-L mechanism and for the 2-step mechanism are over predicted slightly, in comparison to results for the detailed mechanism. A significant disagreement within laminar flame speed is observed between the detailed mechanism and the J-L or the 2S-CM2 mechanism (Figure 26 bottom graph). These reduced mechanisms were evaluated for fuel-air flames and this probably explains such a big divergence, when they are employed in oxy-fuel combustion calculations. Likewise in the conventional combustion simulation with reduced mechanisms (Fig. 7), the oxy-fuel calculation of S_L using the J-L mechanism preserves proper curve shape for different equivalence ratios, as well for the 2S-CM2 mechanism laminar flame speed is overestimated for fuel-rich mixtures.

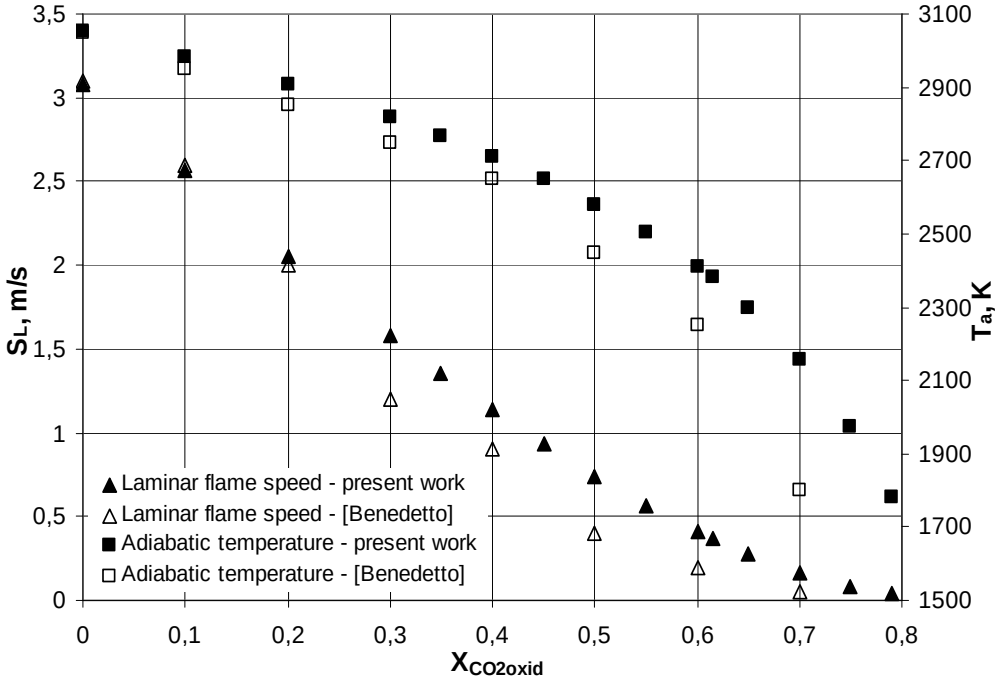

Figure 23: Laminar flame speed and adiabatic flame temperature plotted against CO_2 mole fractions in oxidizer. Results obtained by Benedetto et al. [2] (blank marks) and gained in present work during simulation of flame with GRI Mech (filled marks); $p_0 = 1bar$, $T_0 = 300K$, $\phi = 1,0$.

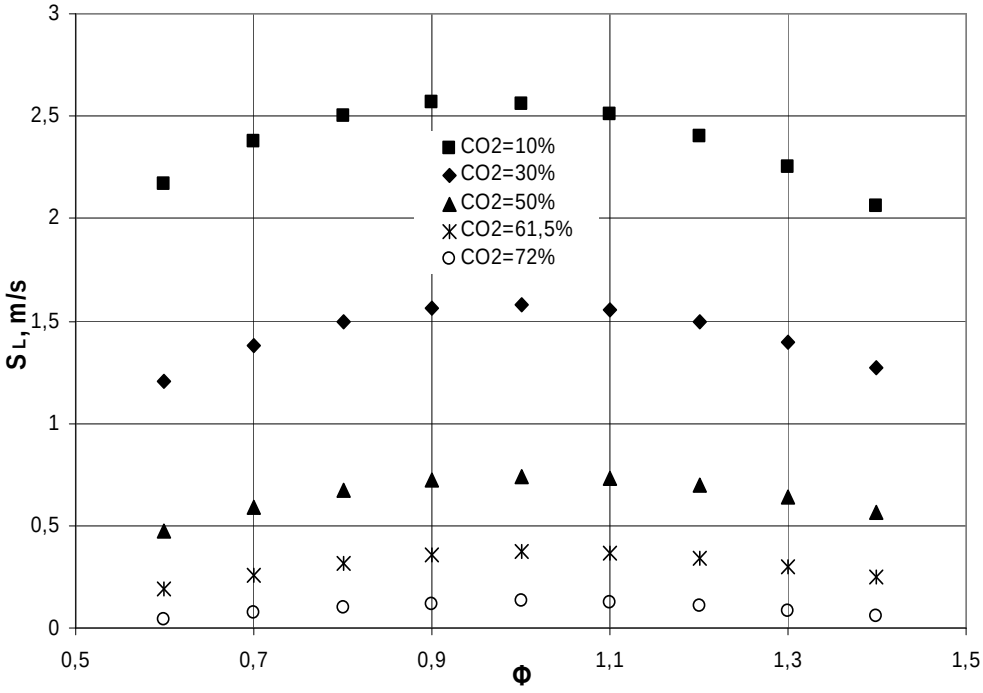

Figure 24: Laminar flame speed for a variety of CO_2 mole fraction in oxidizer plotted against equivalence ratio; $p_0 = 1bar$, $T_0 = 300K$, GRI Mech.

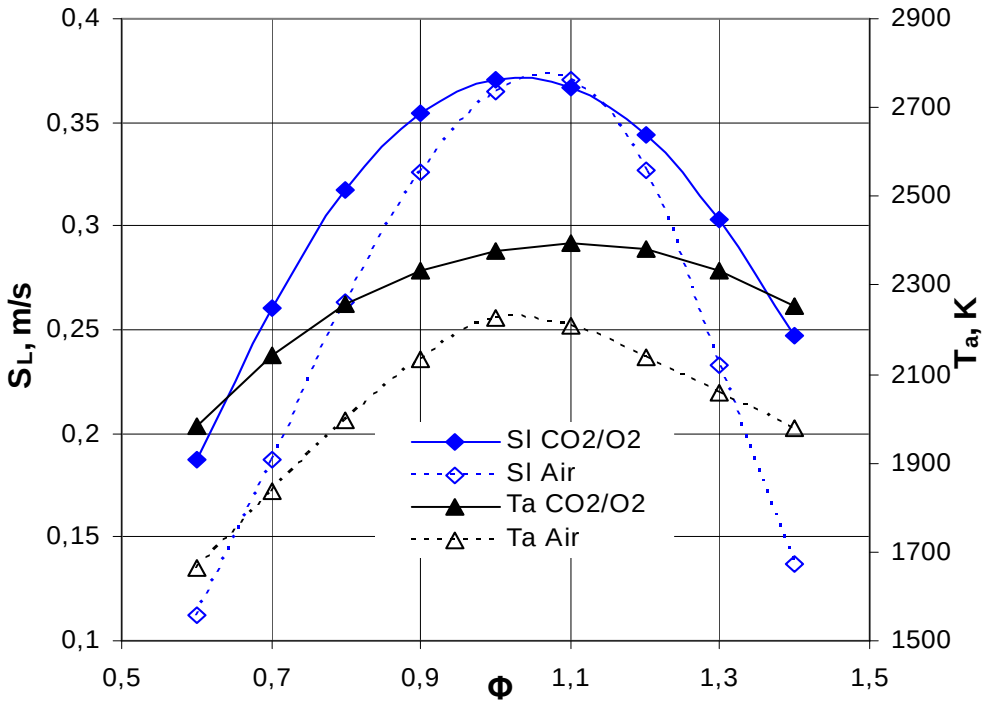

Figure 25: Laminar flame speed and adiabatic flame temperature plotted against equivalence ratio for conventional and for oxy-fuel combustion; $p_0 = 1bar$, $T_0 = 300K$, GRI Mech.

To improve the precision of reduced mechanisms, parameters from the Arrhenius equation (Eq. (13)) were readjusted (Tables 5, 6). For the J-L mechanism two reactions have a major impact on the laminar flame speed: reactions 1 and 3 in Table 3. For both 2S-CM2-JB2 and J-L-JB mechanisms the agreement was improved considerably, however for a fuel-rich mixture the difference between the detailed mechanism and reduced ones is still relatively big, especially for the 2S-CM2-JB2 mechanism. The difference is increasing with increasing equivalence ratio. When for the J-L-JB mechanism this difference can be neglected, for the 2S-CM2-JB2 mechanism the pre-exponential factor adjustment has to be used (Eq. (15), Table 4) .

The similar flame speed for the conventional and the oxy-fuel combustion is not the only criterion considered in this work. Similar flame temperature profiles and gas concentration levels were acquired by Andersson and Johnsson, during experiments, for 27% of molecular oxygen in the oxidizer [4]. For this reason, the simulation of methane combustion in the oxidizer mixture of O_2=0,28/CO_2=0,78 was also performed, in order to match the laminar flame profiles for the detailed mechanism and two reduced ones.

The same procedure of calculations was carried out as for the case with 28% of oxygen in the oxidizer. A better agreement in values of the adiabatic temperature for the detailed mechanism and reduced ones were obtained (Fig. 27) than for a case with 61,5% of CO_2 in the oxidizer (Fig. 26). This was observed, because the lower temperature due to a lower oxygen concentration the lesser temperature divergence between different oxidation mechanisms. Values of the laminar flame speed, for reduced mechanism, were overestimated strongly in comparison to the GRI Mech calculations. To improve the convergence and not to create new mechanisms, the same reduced schemes (J-L-JB and 2S-CM2-JB2) were used (Tables 5, 6). Nevertheless, after readjustment of Arrhenius parameters, a quite good agreement for S_L could be observed, for various oxidation mechanisms during the combustion simulation of fuel-lean and stoichiometric mixtures. Nevertheless, for fuel-rich mixtures, for 2S-CM2-JB2 mechanism a disagreement with the GRI Mech scheme was found, for that reason, a new 2-step scheme with PEA was created (2S-CM2-JB3).

Figure 28 presents calculated values of S_L for GRI Mech, 2S-CM2-JB2 and 2S-CM2-JB3 mecha-

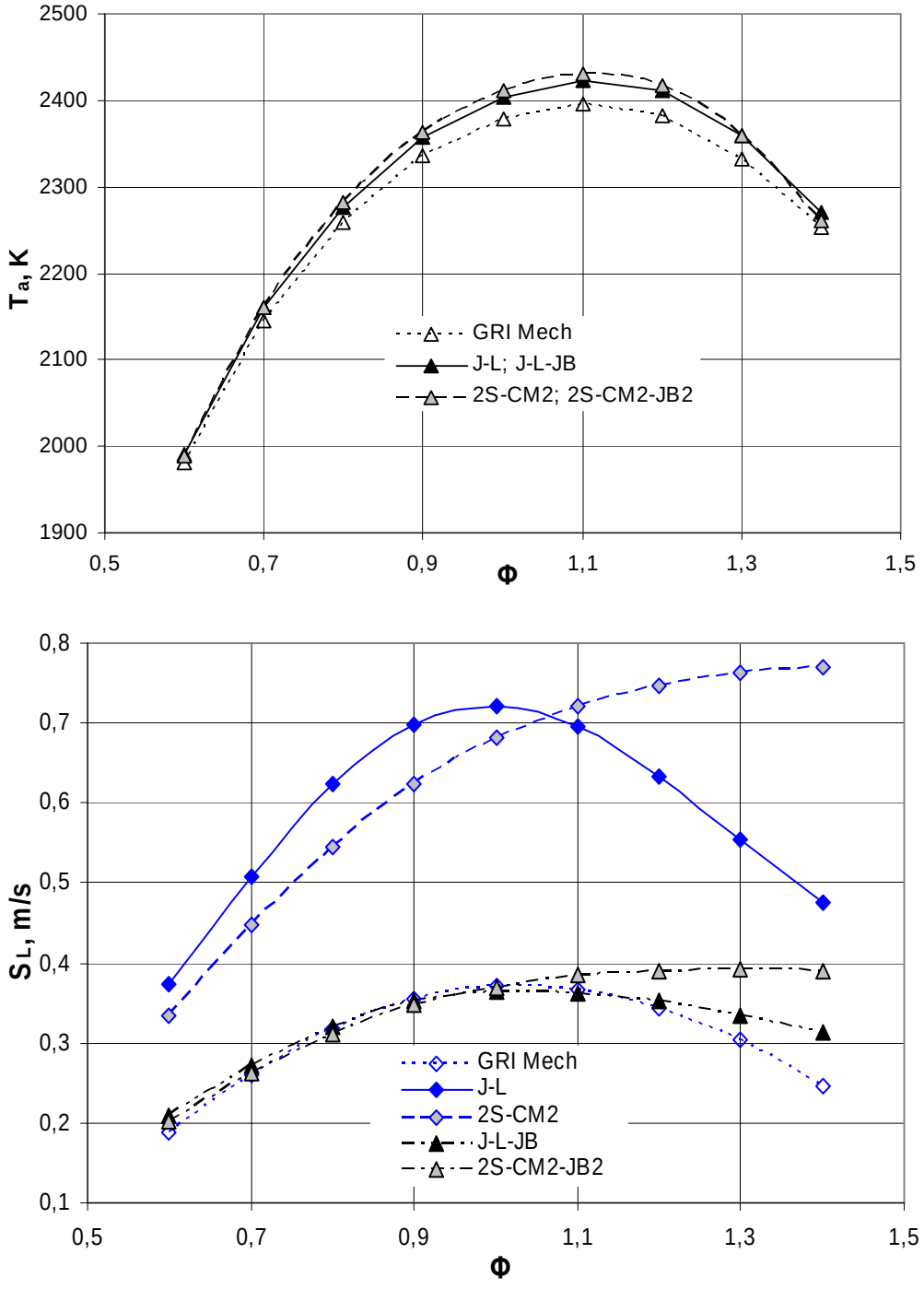

Figure 26: Comparison of the laminar flame speed and the adiabatic temperature results obtained for the detailed mechanism, the original J-L mechanism, the original 2-step mechanism and readjusted ones (J-L-JB and 2S-CM2-JB2) for 38,5% of O_2 in the oxidizer; $p_0 = 1bar$, $T_0 = 300K$.

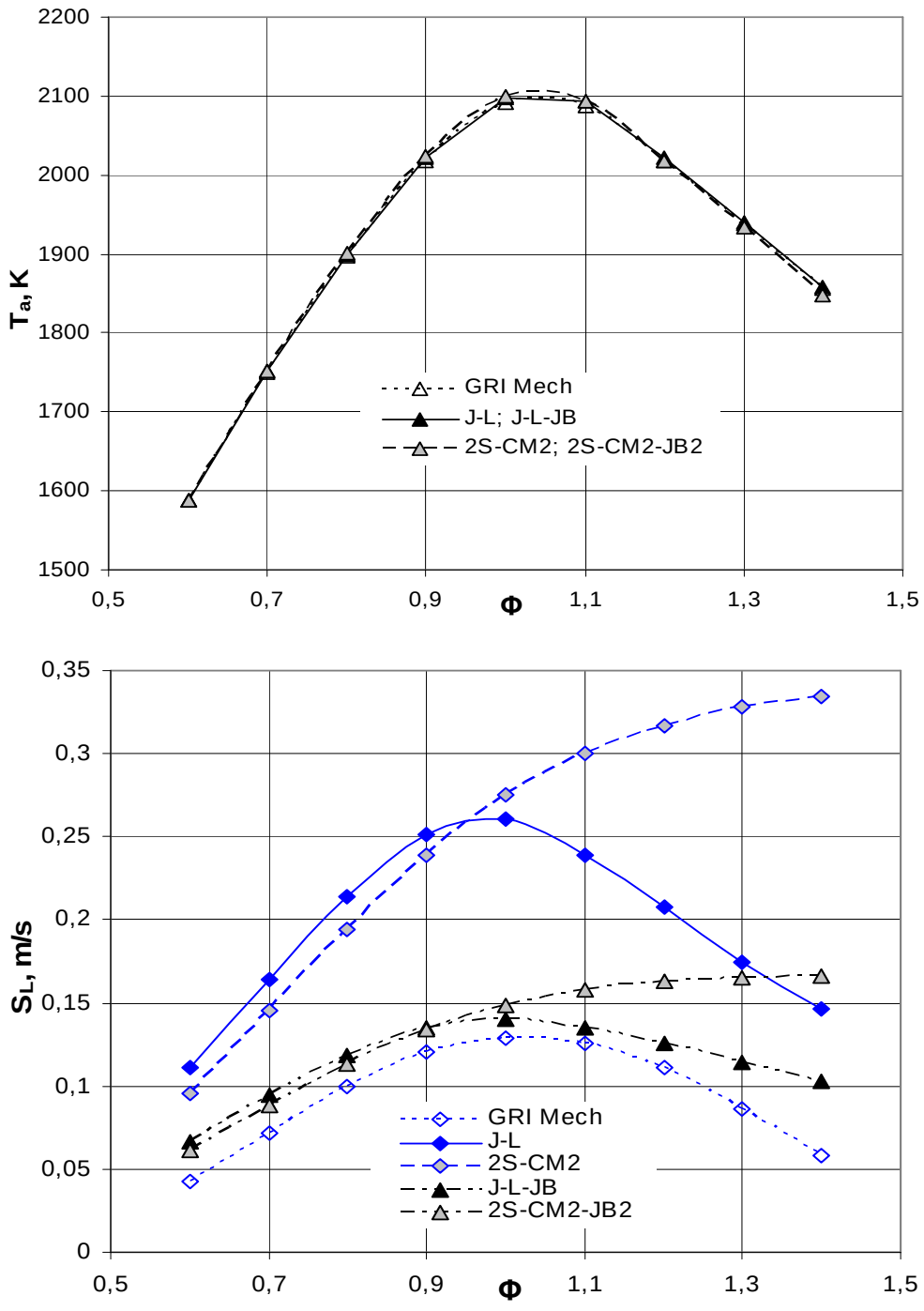

Figure 27: Comparison of the laminar flame speed and the adiabatic temperature results obtained for the detailed mechanism, the original J-L mechanism, the original 2-step mechanism and readjusted ones (J-L-JB and 2S-CM2-JB2) for 28% of O_2 in the oxidizer; $p_0 = 1bar$, $T_0 = 300K$.

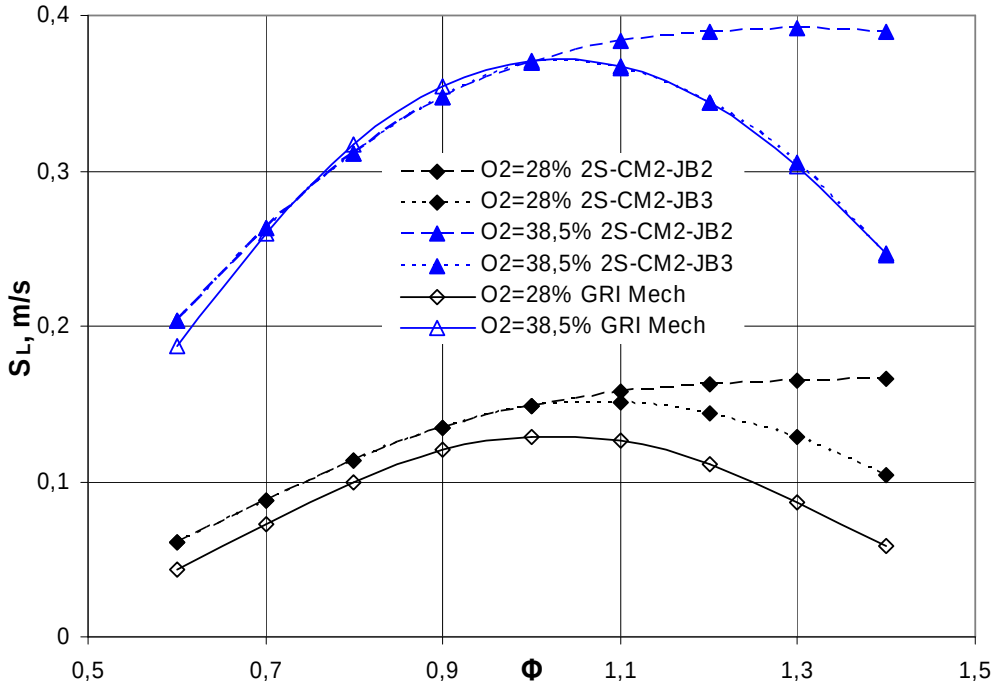

Figure 28: Results comparison of the laminar flame speed values computation for GRI Mech, 2S-CM2-JB2 and for2S-CM2-JB3 plotted against equivalence ratio; $p_0 = 1bar$, $T_0 = 300K$.

nisms. For oxidizer with 38,5% of oxygen a very good agreement between the GRI Mech and 2S-CM2-JB3 is achieved, after employing PEA, for a fuel-rich conditions.
Taking into account the case with 28% of O_2 in the oxidizer, the agreement is only sufficient due to the fact, that PEA function as well as 2S-CM2-JB2 mechanism was created for the oxidizer containing 38,5% of O_2.

One-dimensional stretched premixed laminar flames

The simulations of $CH_4/CO_2/O_2$ one-dimensional stretched premixed laminar flames were performed similarly to methane-air conventional combustion computations. Very good agreement within profiles of velocity and volumetric heat release was found for 2S-CM2-JB2, J-L-JB and GRI Mech schemes, however the maximum mixture velocity as well as the heat release peak are slightly larger for the 2-step and the 4-step mechanism than for GRI Mech (Fig. 30 top graph). Peaks of carbon monoxide and molecular hydrogen mole fractions are under predicted when 2S-CM2-JB2 and J-L-JB mechanisms are employed in calculations (Fig. 30 bottom graph).

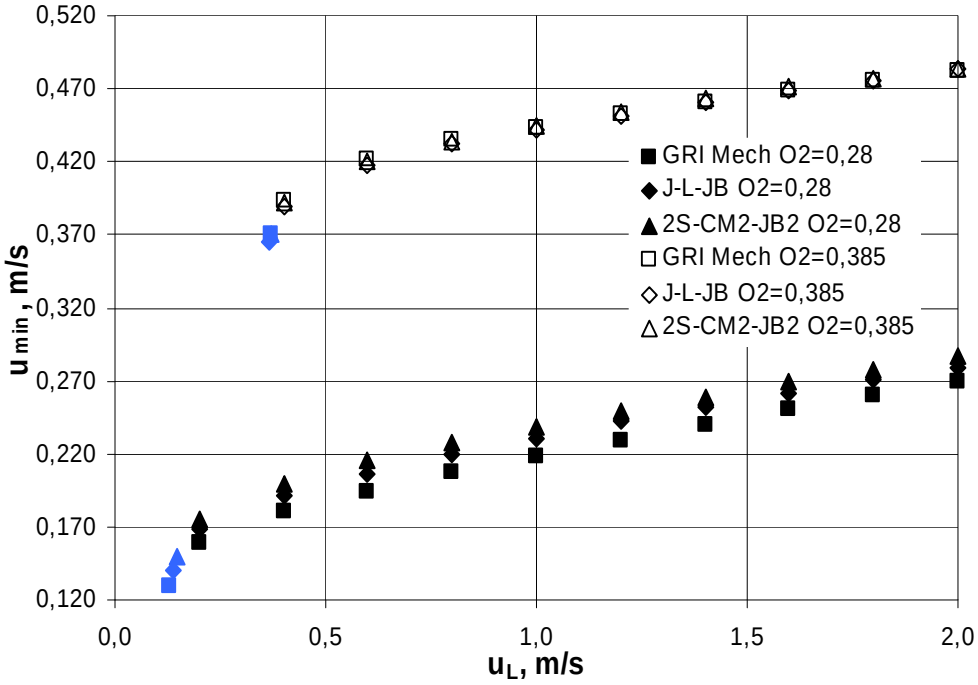

Figure 29: Minimum mixture velocity plotted against inlet velocity for $CH_4/CO_2/O_2$ flames for different oxidation mechanisms for $p_0 = 1bar$, $T_0 = 300K$, $\Phi = 1$; Highlighted marks for $u_L = u_{min}$ are calculated using 1D simulation of freely propagating laminar flame.

The dependency behavior between minimum speed of mixture and inlet velocity are similar to results obtained for a case with $CH_4/N_2/O_2$; a linear dependence were found for a higher u_L values, for both cases with 38,5% and 28% of O_2 in the oxidizer (Fig. 29). Very good conformity for the case with O_2=38,5% in the oxidizer for three considered mechanism was obtained. For the case with O_2=28% in the oxidizer, 2S-CM2-JB2 and J-L-JB2 the minimum mixture velocity (u_{min}) was overestimated slightly in comparison with detailed mechanism.

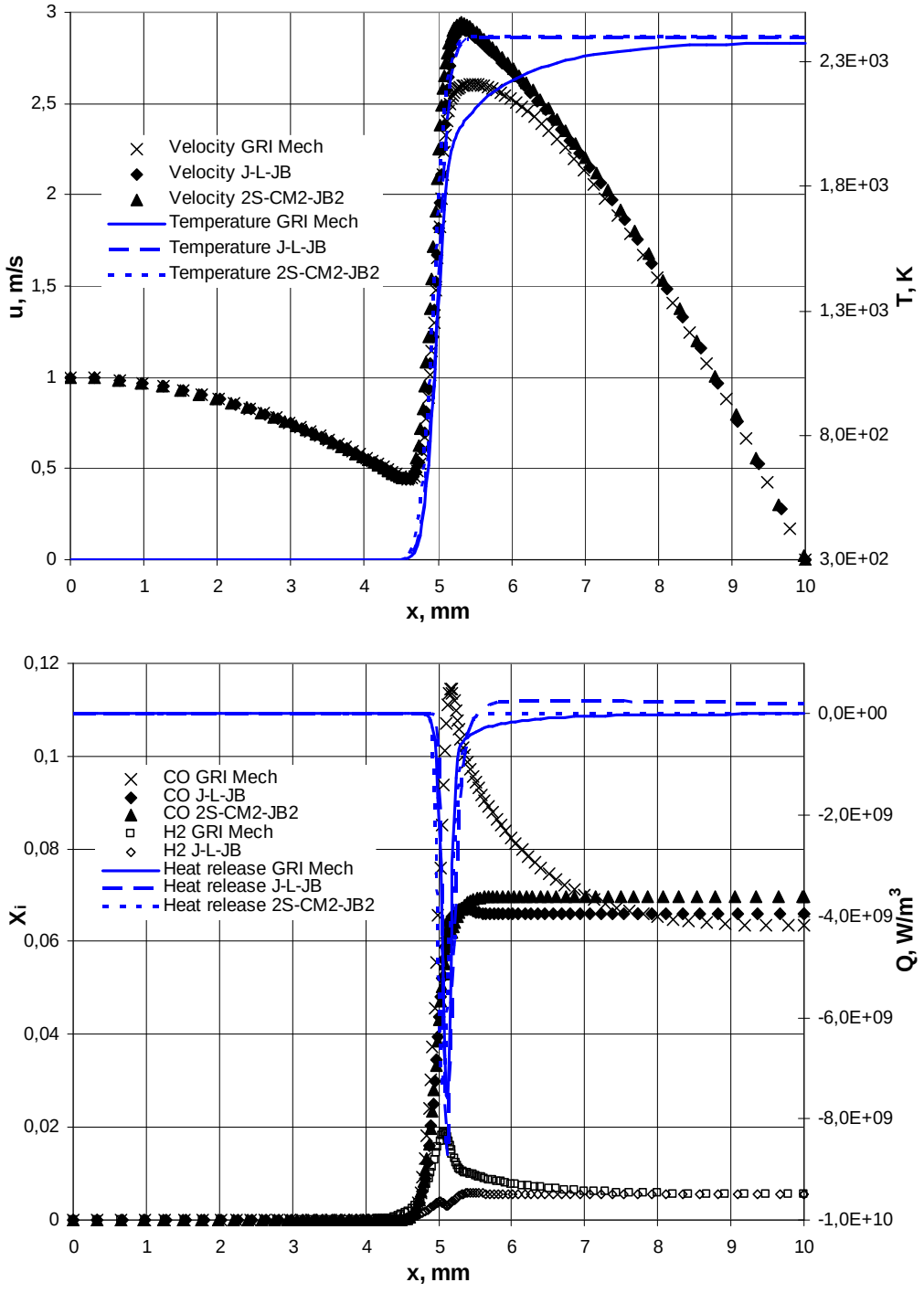

Figure 30: Species, temperature, velocity and heat release profiles for $CH_4/CO_2/O_2$ flames for different oxidation mechanisms for $p_0 = 1bar$, $T_0 = 300K$, $\Phi = 1$, $u_L = 1m/s$, $X_{CO_2}^{oxid} = 0,615$.

One-dimensional stretched diffusion laminar flames

Simulations of $CH_4/CO_2/O_2$ one-dimensional stretched diffusion laminar flames were performed similarly to methane-air conventional combustion computations for the GRI Mech and the 2S-CM2. Results in this chapter are presented for CO_2 in the oxidizer equal to $0,615$.
Very good agreement within profiles of CH_4, O_2, H_2O mole fractions and velocity was found for 2S-CM2-JB2 and GRI Mech schemes, for a strain rate $\kappa = 100$ (Fig. 31 32). Nevertheless, the difference in temperature, heat release, fuel destruction rate and mole fractions of carbon dioxide and carbon monoxide was noticed, as it was observed for methane-air diffusion flames.

The definition of the mixture fraction, because of the oxidizer composition (CO_2/O_2), could not be defined in simple way using atoms of carbon, therefore, the theoretical definition was employed in postprocessing of outcomes (Equation (8)). The mixture fraction plotted against coordinates shows the disturbance of the tendency at the area, where the reactions proceed with the highest intensity (for $z_st \approx 0,073$), especially for the detailed mechanism simulation (Fig. 32 bottom graph).

Similar conclusion can be drawn, as for a conventional combustion case, that absolute value of the integrated fuel reaction rate is increasing with increasing strain rate (Figure 33). For very low strain rates, the difference between values of this quantity, for the GRI Mech scheme and the 2S-CM2-JB2 mechanism, becomes negligible.

A good agreement between results obtained for the GRI Mech, the 2S-CM2-JB2 and equilibrium calculations was found, for the mixture fraction lower than stoichiometric value of this quantity (Figure 34). Nevertheless, for $z_c > z_{st}$ the difference, between results obtained for different calculations, becomes significant, especially for mass fraction of carbon dioxide. Higher temperatures, in comparison with equilibrium calculations, were obtained only for the 2S-CM2-JB2 scheme for wide range of mixture fraction values (Fig. 35). The temperature difference between calculation using the GRI Mech and the 2S-CM2-JB2 reached value $250K$ approximately.

In general, the decrease of the maximum temperatures with increase of stretch rate was found for the GRI Mech, while the maximum temperature obtained for the 2S-CM2-JB2 mechanism was found to be almost insensitive on the strain rate (Figure 36). For the case where oxidizer contained 28% of the O_2, the quenching point were found for strain rate surpassing value of $1901/s$, for detailed mechanism calculations.

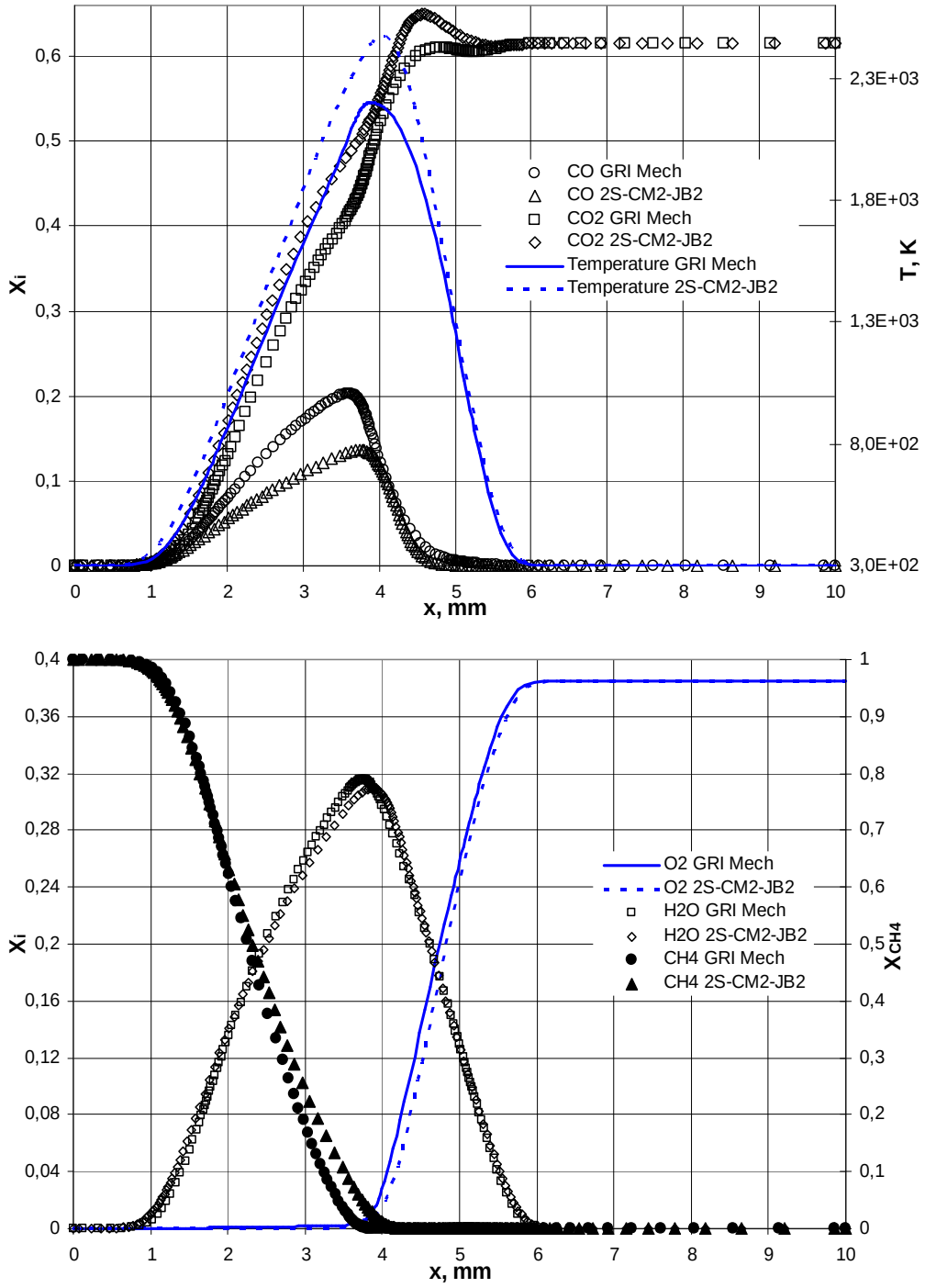

Figure 31: Velocity and heat release profiles comparison for the GRI Mech and the 2S-CM2-JB2; CH_4-O_2=0,385/CO_2=0,615 diffusion flame; $p_0 = 1bar$, $T_0 = 300K$, $\kappa = 100$.

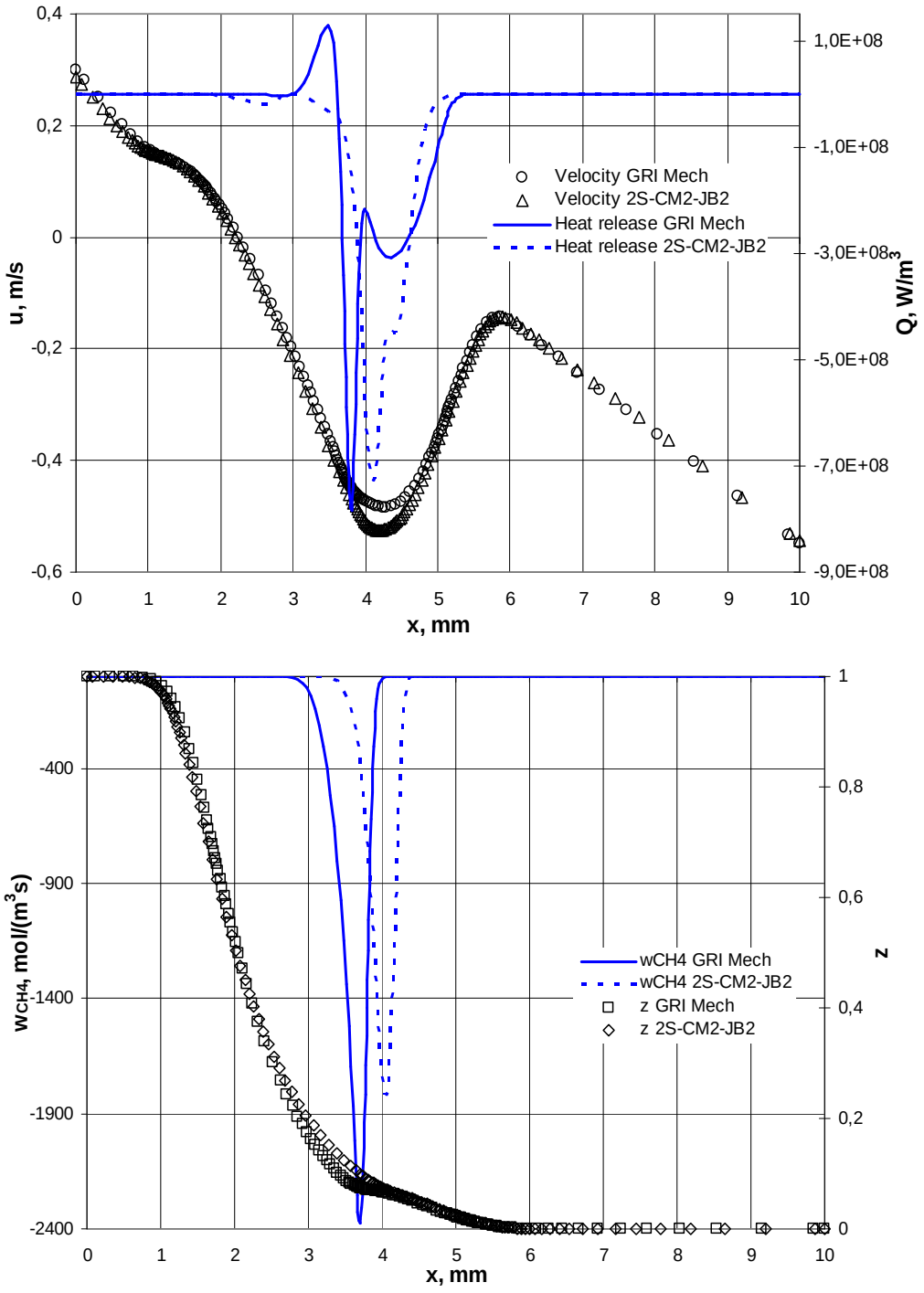

Figure 32: Velocity, heat release, fuel destruction rate and mixture fraction profiles comparison for the GRI Mech and the 2S-CM2-JB2; CH_4-O_2=0,385/CO_2=0,615 diffusion flame; $p_0 = 1bar$, $T_0 = 300K$, $\kappa = 100$.

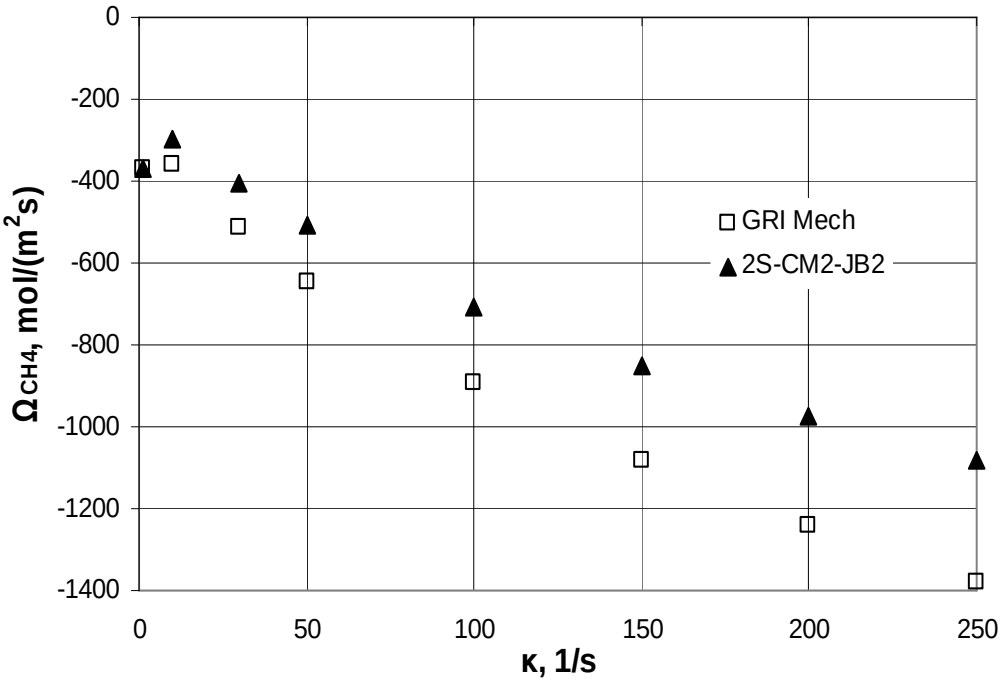

Figure 33: Integrated fuel reaction rates plotted against strain rates for the GRI Mech and the 2S-CM2-JB2; CH_4-O_2=0,385/CO_2=0,615 diffusion flame; $p_0 = 1bar$, $T_0 = 300K$.

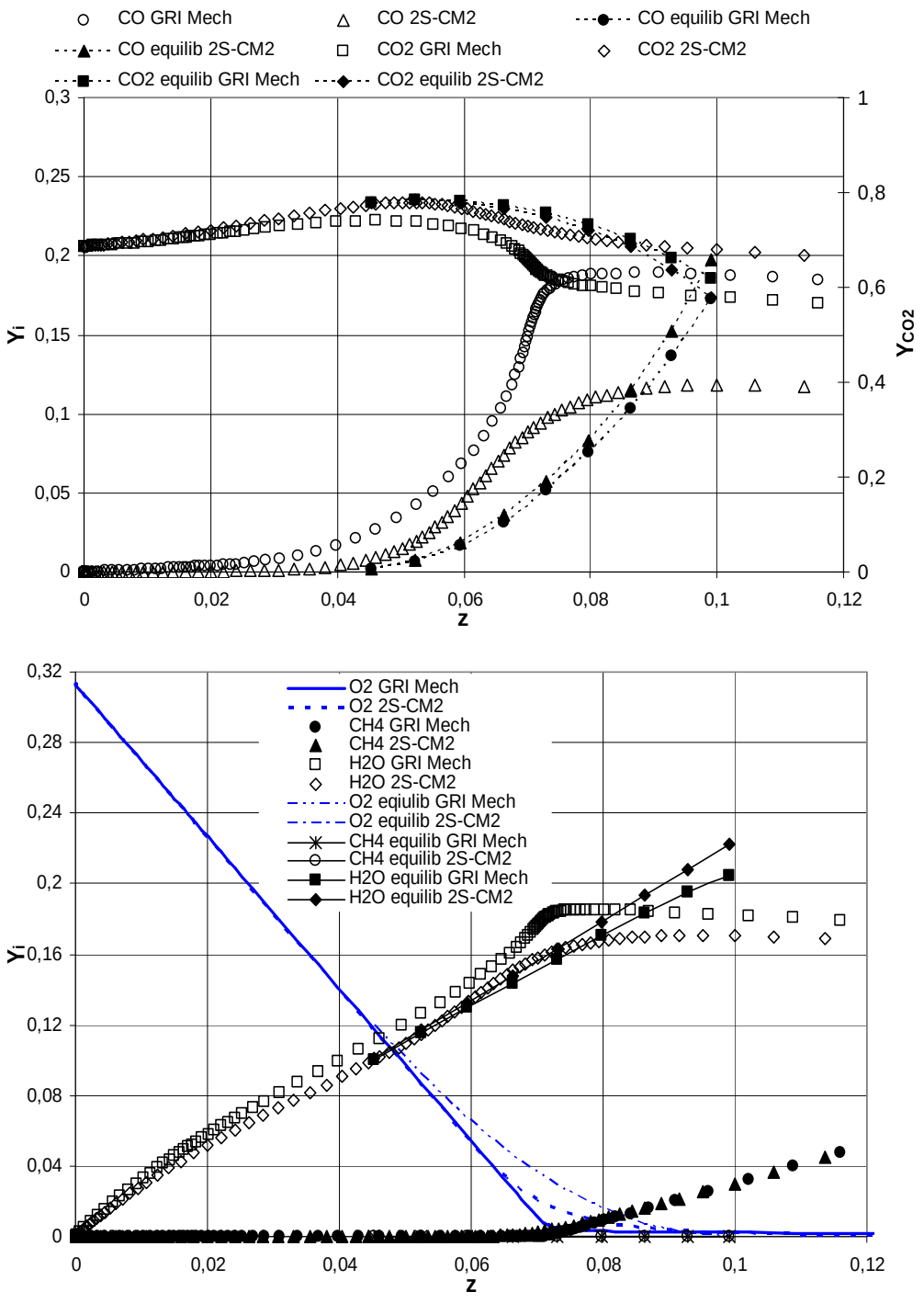

Figure 34: Species mass fractions plotted against mixture fraction for the GRI Mech, the 2S-CM2-JB2 and evaluated from equilibrium calculations; CH_4-O_2=0,385/CO_2=0,615 diffusion flame; $p_0 = 1bar$, $T_0 = 300K$, $\kappa = 100$.

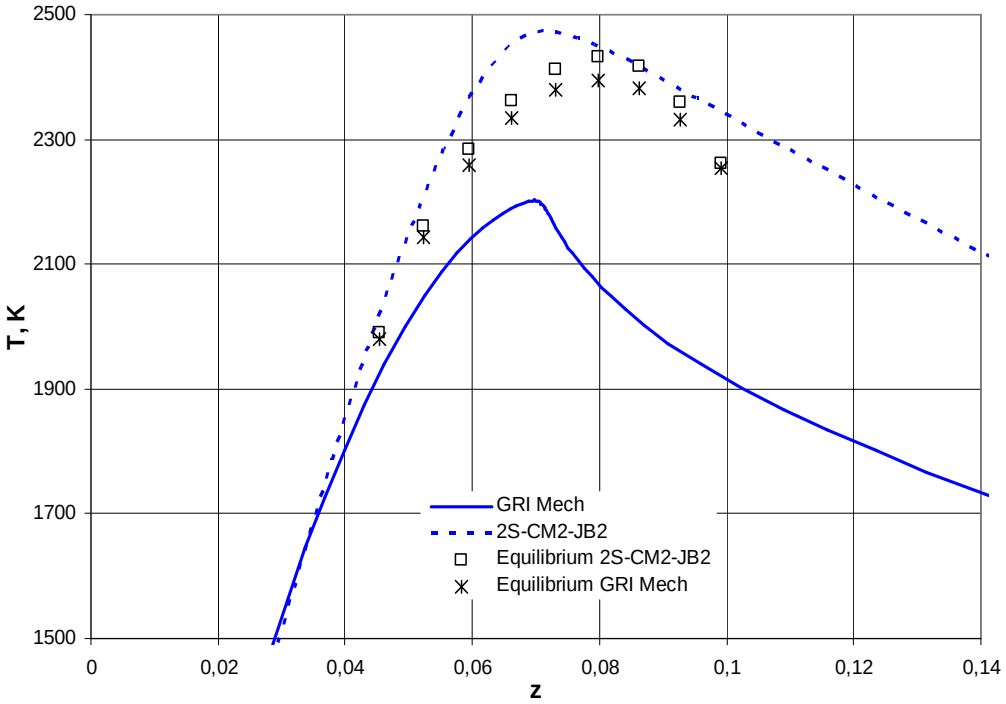

Figure 35: Temperature plotted against mixture fraction for the GRI Mech, the 2S-CM2-JB2 and evaluated from equilibrium calculations; CH_4-O_2=0,385/CO_2=0,615 diffusion flame; $p_0 = 1bar$, $T_0 = 300K$, $\kappa = 100$.

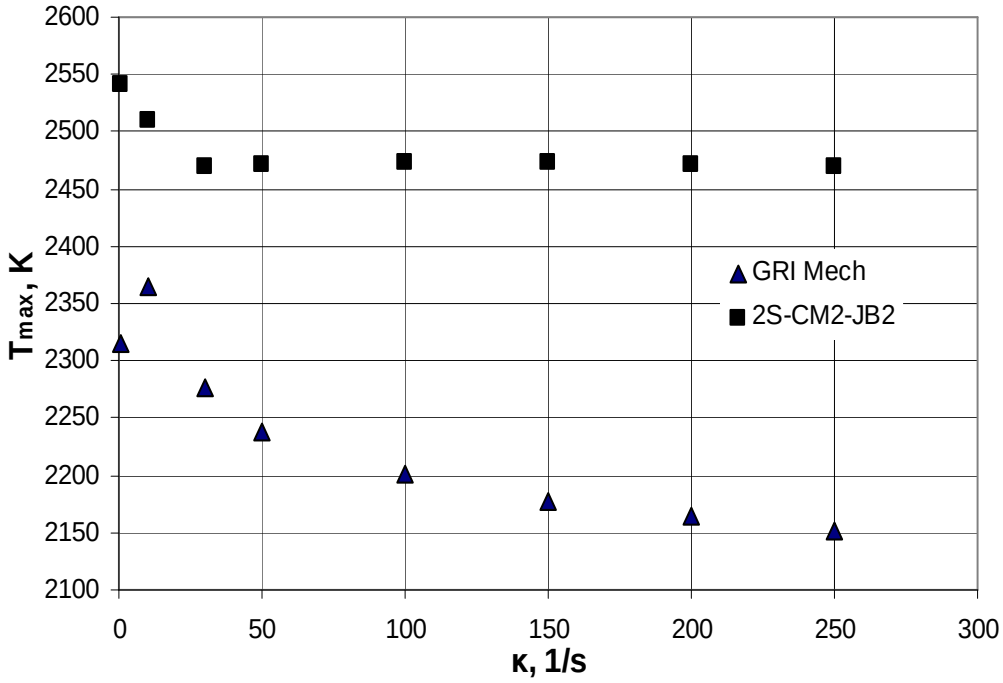

Figure 36: The comparison of the maximum temperature plotted against stretch rate for the GRI Mech and the 2S-CM2-JB2; CH_4-O_2=0,385/CO_2=0,615 diffusion flame; $p_0 = 1bar$, $T_0 = 300K$.

CONCLUSIONS

Two reduced mechanisms (2S-CM2 and J-L) have been tested for a conventional air-methane combustion. Whereas, existing (2S-CM2 and J-L) schemes and refined ones (2S-CM2-JB2 and J-L-JB) were verified using detailed chemistry computations, for specified oxy-fuel conditions.

Results for the air-methane case, obtained for the J-L scheme and for GRI Mech, are in general in better agreement than those evaluated for the 2S-CM2. However, the laminar flame speed obtained for the 2S-CM2 scheme agreed more with results for the GRI Mech than the J-L mechanism, especially when at the rich side of the flame, for the 2-step scheme, a pre-exponential factor adjustment is employed (2S-CM2-JB1). Auto-ignition delay times obtained for both the J-L as well as for the 2S-CM2 are significantly shorter than this quantity obtained for the GRI Mech, thus can be concluded that highly reduced schemes are not able to predict this parameter. The equilibrium calculations have shown that because of considerable overestimation of the adiabatic temperatures for the one-step scheme, this mechanism cannot be used with success in modeling of real processes. Diffusion flames for a conventional methane-air combustion show a good agreement between detailed mechanism calculations and the 2S-CM2 scheme for some of the major species excluding CO_2 and CO.

A large disagreement between detailed chemistry calculations, using the GRI Mech, and results obtained for J-L and 2S-CM2 global schemes, for the oxy-fuel combustion, was found for freely propagating 1D laminar premixed flames. Therefore, two new major schemes were evaluated (2S-CM2-JB2 and J-L-JB). Verification of new schemes was performed in order to obtain similar values of laminar flame speeds for air-methane computations, what were achieved for CO_2 mole fraction in the oxidizer equal to 0,615. However, the usefulness of those schemes were also tested for CO_2 mole fraction in the oxidizer, which insures similar thermal conditions to those, which are present during combustion of methane in air. The prediction of laminar flame speeds were improved significantly, when new schemes for the oxy-methane combustion were employed in simulations.
Similarly, to the air-methane case, the ignition delay times could not be predicted correctly by the 2S-CM2-JB2 scheme as well as by the J-L-JB mechanism. The prediction of the minimum velocity, which was an important quantity for premixed stretched laminar flames, was in very good agreement, for two different oxidizer compositions, at near stoichiometric conditions. A sufficient agreement was also found for diffusion flames, for the GRI Mech mechanism and the 2S-CM2-JB2 scheme, especially for fuel-lean side of the flame.

Generally, modified schemes improved the agreement with the detailed mechanism considerably, for both considering compositions of the oxidizer.

ACKNOWLEDGMENTS

The work presented in this report has been performed at CERFACS (The European Center for Research and Advanced Training in Scientific Computation) and at IMFT (Institut de Mecanique des Fluides de Toulouse) in Toulouse in France. The research activity was supported by the Marie Curie Host Fellowships for Early Stage Research Training within the framework of the ECComET (Efficient and Clean Combustion Experts Training).
I would like to thank my supervisor Professor Thierry Poinsot for his continuous support and helpful suggestions during my training. I also would like to thank my second supervisor Laurent Selle for his help.
I must mention Benedetta Franzelli, who gave me apposite suggestions regarding my calculations.
Finally, I would like to thank to all who gave me any help concerning my work.

References

[1] *Cosilab combustion simulation laboratory manual, version 2.0.*

[2] E. Salzano F. Cammarota G. Russo A. Di Benedetto, V. Di Sarli, *Explosion behavior of ch4/o2/n2/co2 and h2/o2/n2/co2 mixtures*, International Journal of Hydrogen Energy **34** (2009), 6970 6978.

[3] T. Faravelli E. Ranzi C. Candusso A. Frassoldati, A. Cuoci and D. Tolazzi, *Simplified kinetic schemes for oxy-fuel combustion*, 1st International Conference on Sustainable Fossil Fuels for Future Energy, 2009.

[4] K. Andersson and Filip Johnsson, *Flame and radiation characteristics of gas-fired o2/co2 combustion*, Fuel **86** (2007), 656668.

[5] C. K. Law B. H. Chao, F. N. Egolfopoulos, *Structure and propagation of premixed flame in nozzle-generated counterflow*, Combustion and Flame **109** (1997), 620–638.

[6] G. Boudier, *Methane/air flame with 2-step chemistry: 2s ch4 cm2*, Tech. report, CERFACS, 2007.

[7] I. Gokalp D. F. Kurtulus C. Cohea, Ch. Chauveau, *Co2 addition and pressure effects on laminar and turbulent lean premixed ch4 air flames*, Proceedings of the Combustion Institute **32** (2009), 18031810.

[8] C. K. Law C. J. Sung and J. Y. Chen, *An augmented reduced mechanism for methane oxidation with comprehensive global parametric validation*, Twenty-Seventh Symposium (International) on Combustion/The Combustion Institute, 1998.

[9] James F. Driscoll, *Turbulent premixed combustion: Flamelet structure and its effect on turbulent burning velocities*, Progress in Energy and Combustion Science **34** (2008), 91134.

[10] M. Frenklach N. W. Moriarty B. Eiteneer M. Goldenberg C. T. Bowman R. K. Hanson S. Song W. C. Gardiner Jr. V. V. Lissianski G. P. Smith, D. M. Golden and Z. Qin, *Gri mech 3.0 http://www.me.berkeley.edu/gri-mech/*.

[11] L.Y.M. Gicquel, *How to introduce new fuels in avbp*.

[12] X. J. Gu, M. Z. Haq, M. Lawes, and R. Woolley, *Laminar burning velocity and markstein lengths of methane-air mixtures*, Combust. Flame **121** (2000), 41–58.

[13] J.P. Holman, *Thermodynamics 3rd edition*, McGraw-Hill, 1980.

[14] T. Giselsson J. Andersen, Ch. L. Rasmussen and P. Glarborg, *Global combustion mechanisms for use in cfd modeling under oxy-fuel conditions*, Energy & Fuels **23** (2009), 13791389.

[15] O. B. Kwon E. J. Lee J. H. Yun J. S. Kim, J. Park and S. I. Keel, *Preferential diffusion effects in opposed-flow diffusion flame with blended fuels of ch4 and h2*, International Journal of Hydrogen Energy **33** (2008), 842 850.

[16] W. P. Jones and R. P. Lindstedt, *Global reaction schemes for hydrocarbon combustion*, Combust. Flame **73** (1988), 222–233.

[17] Andrzej Kowalewicz, *Podstawy procesow spalania*, Wydawnictwa Naukowo-Techniczne, 2000.

[18] T. Boushaki B. Ferret L. Selle, Y. Dhue and T. Poinsot, *Experimental and numerical study of the accuracy of flame-speed measurements in bunsen burner*, Sixth Mediterranean Combustion Symposium MCS 6, 2009.

[19] G. Lacaze, *Arrhenius kinetic parameters for a reversed equilibrium reaction*, Tech. report, CERFACS, 2006.

[20] D. Thevenin O. Gicquel and N. Darabiha, *Influence of differential diffusion on super-equilibrium temperature in turbulent non-premixed hydrogen/air flames*, Flow, Turbulence and Combustion **73** (2004), 307321.

[21] Ryszard Petela, *Paliwa i ich spalanie cz. ii spalanie*, Dzial Wydawnictw Politechniki Slaskiej, 1982.

[22] N. Peters and R. J. Kee, *The computation of stretched laminar methane-air diffusion flames using a reduced four-step mechanism*, Combustion and Flame **68** (1987), 17–29.

[23] T. Poinsot and D. Veynante, *Theoretical and numerical combustion*, R.T. Edwards, 2nd edition, 2005.

[24] B. Rogg R. S. Cant and K. N. C. Bray, *On laminar flamelet modelling of the mean reaction rate in a premixed turbulent flame*, Combustion Science and Technology **69** (1990), 53–61.

[25] J. Quinard S. G. Davis and G. Searby, *Determination of markstein numbers in counterflow premixed flames*, Combustion and Flame **130** (2002), 112–122.

[26] J. Szargut, *Termodynamika techniczna dla kierunkow nieenergetycznych*, Wydawnictwo Politechniki Slaskiej, 1969.

[27] Z. Xu T. Takagi and M. Komiyama, *Preferential diffusion effects on the temperature in usual and inverse diffusion flames*, Combustion and flame **106** (1996), 252–260.

[28] J. Tomeczek, *Spalanie i plomienie gazowe*, Dzial Wydawnictw Politechniki Slaskiej, 1982.

[29] C. M. Vagelopoulos and F. Egolfopoulos, *Direct experimental determination of laminar flame speeds*, 27th Symp. (Int.) on Combustion, The Combustion Institute, Pittsburgh, 1998, pp. 513–519.

[30] C. Westbrook and F. Dryer, *Simplified reaction mechanism for the oxidation of hydrocarbon fuels in flames*, Combust. Sci. Tech. **27** (1981), 31–43.

[31] A. C. Zambon and H. K. Chelliah, *Explicit reduced reaction models for ignition, flame propagation, and extinction of c2h4/ch4/h2 and air systems*, Combustion and Flame **150** (2007), 71–91.